https://doi.org/10.5194/wes-2019-108
Preprint. Discussion started: 17 January 2020

eawe european academy of wind energy
Open Access WIND ENERGY SCIENCE DISCUSSIONS

Clustering wind profile shapes to estimate airborne wind energy production

Mark Schelbergen[1], Peter C. Kalverla[2], Roland Schmehl[1], and Simon J. Watson[1]

[1]Faculty of Aerospace Engineering, Delft University of Technology, Kluyverweg 1, 2629 HS Delft, The Netherlands
[2]Meteorology and Air Quality Section, Wageningen University, PO box 47, 6700 AA Wageningen, The Netherlands

Correspondence: Mark Schelbergen (m.schelbergen@tudelft.nl)

Abstract. Airborne wind energy (AWE) systems typically harness energy in an altitude range up to 500 m above the ground. To estimate the annual energy production (AEP), measured wind speed statistics close to the ground are commonly extrapolated to higher altitudes, introducing substantial uncertainties. This study proposes a clustering procedure for obtaining wind statistics for an extended height range from reanalysis data or long-term LiDAR measurements that include the vertical variation of the wind speed and direction. K-means clustering is used to identify a set of prevailing wind profile shapes that characterise the wind resource. The methodology is demonstrated using the Dutch Offshore Wind Atlas and LiDAR observations for the locations of the met masts IJmuiden and Cabauw, 85 km off the Dutch coast in the North Sea and in the center of the Netherlands, respectively. The resulting wind profile shapes and the corresponding temporal cycles, wind properties, and atmospheric stability are in good agreement with literature. Finally, it is demonstrated how a set of wind profile shapes and their statistics can be used to estimate the AEP of a pumping AWE system. For four or more clusters, the site specific AEP error is within a few percent of the converged value.

1 Introduction

Airborne wind energy (AWE) systems use tethered flying devices to harness energy at higher altitudes than tower-based wind turbines, typically in a range up to 500 m, where wind is generally stronger and more persistent. For estimating annual energy production (AEP), wind speed statistics in the full operational height range of the AWE system are commonly approximated by extrapolating the wind speed distribution close to the ground to higher altitudes using either the wind profile power law or the logarithmic profile (e.g., Heilmann and Houle, 2013). This way of representing the wind resource introduces substantial uncertainties since the aforementioned wind profile relationships are not strictly valid beyond the surface layer (up to around 200 m) and deviating profiles are likely to occur.

The power law is a simple empirical relationship obtained from a large amount of measurement data, often far below 500 m (Peterson and Hennessey, 1978), and does not offer enough flexibility to describe the variety of measured wind profiles (e.g., Park et al., 2014). The logarithmic wind profile is based on physical arguments, but it rests on a number of assumptions that are violated in practice (e.g., Optis et al., 2014). Both wind profile relationships neglect the variation of the wind direction with height and assume that wind speed increases monotonically with height. In practice, the wind direction can vary substantially

https://doi.org/10.5194/wes-2019-108
Preprint. Discussion started: 17 January 2020

eawe european academy of wind energy
Open Access WIND ENERGY SCIENCE DISCUSSIONS

in the lower 500 m (e.g., Brown et al., 2005; Floors et al., 2015). Recent studies have identified numerous low-level jets, characterised by low level maxima with decreasing wind speed above (e.g., Ranjha et al., 2013; Kalverla et al., 2019). To extend the validity of wind profile relationships to higher altitudes, several modifications have been proposed (e.g., Gryning et al., 2007; Holtslag et al., 2017). However, these theoretical formulations are only validated up to heights relevant for more conventional, tower-based wind turbines.

Alternatively, computationally expensive, brute force calculations of the energy production do not assume any wind profile relationship and are performed using historical wind data for the full operational height range. Bechtle et al. (2019) use ERA5 reanalysis data to map out the wind resource available to AWE systems over a large part of Europe, but do not touch upon the performance calculations. Ranneberg et al. (2018) combine COSMO-DE reanalysis data with power curves for multiple heights, that are independent of the wind profile, to estimate the AEP. This is a valid approach if the system is operating at a nearly constant height. However, the wind profile has to be considered if the system operates in a larger height range, such as flexible-kite AWE system (Van der Vlugt et al., 2019). AEP calculations get more computationally expensive if the wind profile is considered, especially when optimisations are used to maximise the power output for each point in time. Malz et al. (2020b) use MERRA-2 reanalysis data and perform performance optimisations for similar wind profiles sequentially, in an achronological order. This allows the selection of good starting points for the optimisations and reducing the computational time by a factor of 1.5. In a follow-up study, Malz et al. (2020a) use this approach to determine the AEP of an AWE system for 16 locations in Europe. The current state-of-the-art is lacking a methodology that can be confidently used to do fast AEP calculations for a pumping AWE system that sweeps a non-negligible height range.

Previously, clustering techniques have been used for identifying wind profile patterns. Sommerfeld et al. (2019) applies k-means clustering to subdivide stable and unstable wind profile datasets from WRF simulations into two clusters for a location in a mostly flat area in northern Germany. Duran et al. (2019) use self organising maps to characterise vertical wind profile data for two locations (Cabauw in the centre of the Netherlands and FINO-1 in the North Sea, 45 km north of the German/Dutch coast) from WRF simulations using 2300 clusters for forecast verification and investigate diurnal and seasonal cycles in the occurrence of the clusters.

This study proposes a clustering procedure for obtaining wind resource statistics from reanalysis data or long-term LiDAR observations that include the vertical variation of the wind speed and direction. The full spectrum of wind conditions in such a historical dataset is reduced to a small number of prevailing wind profile shapes using clustering. We have chosen an empirical approach for identifying wind profile patterns to ensure that the wind profile shapes are not restricted by physical assumptions. Nevertheless, we try to physically interpret the observed features. In contrast to earlier studies that use clustering, we have clustered normalised vertical wind profiles, since these are often described by wind profile relationships and an even more compact wind resource representation can be obtained. Moreover, the variation of the wind direction with height is included as it affects the operation of an AWE system.

The following paper structure outlines the process of making a fast AEP estimation of an AWE system based on historical wind data. In Sect. 2, the Dutch Offshore Wind Atlas (DOWA), LiDAR, and ERA5 datasets are introduced. In Sect. 3, the data processing and clustering techniques are discussed, complemented by interim results. In Sect. 4, the clustering results

https://doi.org/10.5194/wes-2019-108
Preprint. Discussion started: 17 January 2020

are presented for an off- and onshore location: met mast IJmuiden and Cabauw, using DOWA data. The wind profile shapes that result from the DOWA and LiDAR data are compared for the met mast IJmuiden location. Subsequently, the procedure is applied to 45 other locations at once to generate a generalised set of wind profile shapes that is applicable for an area which includes a wide range of location types. Although the resulting wind resource representation can be used for various applications, it is originally developed for acquiring a more accurate AEP estimation for pumping AWE systems. Section 5 demonstrates how it can be used to estimate the AEP of a flexible-kite AWE system. Furthermore, the required number of wind profile shapes (clusters) for an accurate estimation of the energy production is assessed. Finally, in Sect. 6 the conclusions from this study are summarised.

2 Wind datasets

In principle, datasets containing time series of wind speeds and directions for multiple altitudes can be used as input for the proposed methodology. Both simulated data and measurements can be used. This paper focusses on datasets with at least an hourly temporal resolution allowing the investigation of diurnal cycles. The first commercial AWE initiatives envisage a maximum operational height of 500 m because operation at higher altitudes requires more complex system designs and legislative procedures. Therefore, for the purpose of this paper, it is desirable to have wind data up to this height. The vertical resolution should be adequate to assess the shape of the vertical wind profile with sufficient detail and simulate the AWE system performance. Both long-term LiDAR observations and reanalysis data qualify as input. This study focusses on using reanalysis data, which provides good spatial and temporal coverage. The sparser LiDAR observations are used only for validation at a single location.

A typical offshore location in the North Sea and onshore location in the Netherlands are selected for demonstrating the methodology. The selected offshore location is that of the met mast IJmuiden (MMIJ), which is located 85 km off the Dutch coast in the North Sea. Next to using reanalysis data, the mast's LiDAR observations are used. The selected onshore location is that of the met mast Cabauw (MMC), in the centre of the Netherlands. The area immediately surrounding the mast is flat open grass-land for at least 400 m in all directions and up to 2 km in the dominant wind direction (WSW). Within a radius of 20 km, the terrain is predominantly grass-land and is virtually flat. Only reanalysis data is used for this location. The MMIJ and MMC locations are marked using respectively a cross and square in Fig. 1.

2.1 ERA5

ERA5 is a global reanalysis performed by ECMWF using their integrated forecasting system, which is ECMWF's atmospheric model and data assimilation system. At the time of writing, the data are available from 1979 to the present time (2019). In the near future data will be made available from 1950. The dataset includes hourly modelled values of a large number of atmospheric variables on a 30 km horizontal grid with 137 vertical pressure levels up to a height of roughly 80 km. As the model outputs data at fixed vertical pressure levels, the physical heights are time dependent and interpolation is needed to obtain the wind data for fixed heights as required by the clustering procedure.

https://doi.org/10.5194/wes-2019-108
Preprint. Discussion started: 17 January 2020

eawe european academy of wind energy
Open Access WIND ENERGY SCIENCE DISCUSSIONS

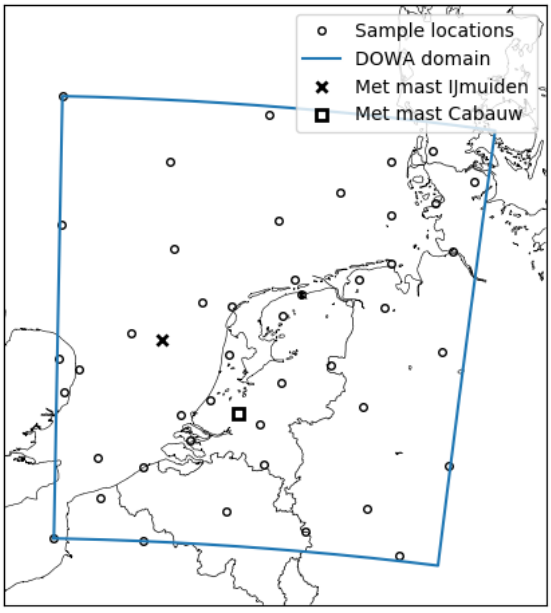

Figure 1. The area under analysis, which covers the Netherlands, a substantial part of the North Sea, and adjoining coastal areas.

The ERA5 dataset allows the characterisation of the long-term wind climatology, for which typically at least 30 years of data are needed. For this work, the ERA5 dataset is only used to assess the atmospheric stability at specific locations. For analysis of the long-term wind speed profiles, we have chosen to use the Dutch Offshore Wind Atlas (DOWA) which is described in the following section.

2.2 Dutch offshore wind atlas

The DOWA is based on the ERA5 reanalysis and downscaled using the mesoscale weather model HARMONIE-AROME (http://www.dutchoffshorewindatlas.nl/). The downscaled reanalysis is performed for 10 years from 2008 until 2017. Hourly values for temperature, wind speed and direction, pressure and relative humidity are made available on 2.5 km grid (217 x 234 points) and 17 heights between 10 and 600 m. The DOWA domain is illustrated in Fig. 1. The higher resolution and the fact that HARMONIE, as opposed to ERA5, is a non-hydrostatic model allows for a better representation of the coastal morphology, land surface heterogeneity and mesoscale circulations such as the sea breeze than is possible than using ERA5 alone. Furthermore, additional observations from routine weather stations, ASCAT satellite retrievals and mode-s ehs aircraft sensors have been assimilated by the HARMONIE model. Validation of the DOWA dataset is available on the DOWA website. Additionally, Kalverla (2019) show that it outperforms ERA5 in terms of wind speed and directional accuracy, as well as the representation of anomalous events such as low-level jets and wind shear.

https://doi.org/10.5194/wes-2019-108
Preprint. Discussion started: 17 January 2020

eawe european academy of wind energy
Open Access WIND ENERGY SCIENCE DISCUSSIONS

2.3 LiDAR observations

LiDAR observations for MMIJ are used to compare results of the clustering procedure using reanalysis data and measurements. Between November 2011 and March 2016, a Zephir 300 continuous-wave LiDAR measured wind speed and direction between 90 and 315 m height at 25 m intervals (Kalverla et al., 2017). ECN post-processed the measurements and published the 10 minute averaged values (http://www.meteomastijmuiden.nl). The samples that exhibit a 180 degree change in wind direction between adjacent or over the span of three height points are discarded. Clock hour averages are calculated from the 10 minute averages when all 6 samples within that hour are available. In this study, the data for 2012 until 2015 are analysed. After this processing, the dataset available for the clustering procedure had a temporal availability of 75 %. Note that the data set is not ideal for performing AEP calculations for AWE systems as it does not go up to 500 m height. Nevertheless, the temporal availability makes it useful for validation purposes.

3 Clustering procedure

This section illustrates the clustering procedure using the DOWA wind data for the MMIJ location. The data is filtered and normalised and its dimensions are reduced using a principal component analysis. Next, the clustering performance is analysed for choosing the number of clusters.

3.1 Preprocessing of the wind data

We study the wind profile shape in its entirety, including both wind speed and direction. Similar to what has been done by Kalverla et al. (2017) and Malz et al. (2020b), to obtain a uniform dataset of wind profile shapes, independent of the prevailing wind speed or direction, the wind speeds are expressed as the (horizontal) components parallel and perpendicular to the reference wind velocity at 100 m for each height. To obtain a procedure that is robust with respect to outliers, each sample is normalised by the 90th percentile of its wind speeds at each height, referred to as the normalisation wind speed.

The normalisation yields representative wind profile shapes for moderate and strong winds. For low wind speeds, eccentric wind profile shapes can be expected due to the normalisation. The wind profiles that have a mean wind speed below 5 $\mathrm{m\,s^{-1}}$ are therefore omitted in the training dataset for the clustering. Note that these profiles are less significant for wind energy systems as they only account for a small part of the AEP. Nonetheless, they are included in the AEP calculation in Sect. 5. Unless stated otherwise, the results presented in Sect. 4 are based on the filtered dataset.

3.2 Principal component analysis of the wind profile shape dataset

Prior to clustering, a principal component analysis (PCA) is commonly used to reduce the dimensionality of a dataset, while preserving most of the variance. This reduces the computational effort and thus speeds up the clustering. The PCA specifies a transformation from the original to the principle component coordinate system, which is orthogonal and has its origin located at the mean of the dataset. The first axis is oriented such that it accounts for most of the variance in the data. Subsequent axes

https://doi.org/10.5194/wes-2019-108
Preprint. Discussion started: 17 January 2020

eawe european academy of wind energy
Open Access WIND ENERGY SCIENCE DISCUSSIONS

are perpendicular to their predecessors and oriented such that they account for as much of the variance as possible. As a result, the last axis accounts for least of the variance.

The mean wind profile shape for the MMIJ is shown in the upper left panel of Fig. 2. The shape exhibits low shear, as expected for an offshore location with low surface roughness for every wind direction. To illustrate the difference with a logarithmic profile representation of the wind environment, a logarithmic profile with a roughness length of $0.0002\ \mathrm{m}$ is fitted to the vertical, normalised wind speed magnitude. The wind speed of the logarithmic profile at height z is:

$$u(z) = \frac{u_*}{\kappa}\left[\ln\left(\frac{z}{z_0}\right) - \Psi\left(\frac{z}{L}\right) + \Psi\left(\frac{z_0}{L}\right)\right], \tag{1}$$

in which u_* is the friction velocity, κ is the von Karman constant, z_0 is the roughness length, Ψ is a stability correction function, and L is the Obukhov length. The following stability correction functions are adopted (Holtslag et al., 2014):

$$\Psi(L \leq 0) = 2\ln\left(\frac{1+x}{2}\right) + \ln\left(\frac{1+x^2}{2}\right) - 2\arctan(x) + \frac{\pi}{2}, \qquad x = \left(1 - 19.3\frac{z}{L}\right)^{\frac{1}{4}},$$

$$\Psi(L \geq 0) = -6.0\frac{z}{L}.$$

The mean shape shows a good fit with an unstable logarithmic profile. The normalised perpendicular wind speed, which is by definition zero for $100\ \mathrm{m}$ height, decreases with height. In accordance with theory, the wind profile rotates in the clockwise direction with height (it veers with height), which can be observed in the hodograph (top-view) of the wind profile shape in the lower left panel of Fig. 2.

The principal components are unit vectors that consist of the relative contributions of the original features (normalised wind speeds for a set of heights). The first two principal components (PC1 and PC2) of the wind profile shape dataset are shown in the second column of Fig. 2. The perpendicular wind speeds have a relatively large contribution to PC1, indicating that the wind veer changes substantially along PC1. This is in contrast to PC2, along which mainly the parallel wind speeds changes.

The features of the dataset are no longer (normalised) physical properties, but contain contributions of all the normalised wind speeds. The third and fourth column of Fig. 2 illustrate how the wind profile shapes vary along the corresponding principal component. They illustrate that PC1 mostly contains information related to the wind veer (i.e. the change of wind direction with height), while PC2 mostly contains information about wind shear (i.e. the change of wind speed with height).

For clustering purposes, the approximation error is typically considered acceptable when using a reduced dataset that retains between 90–99 % of the variance. Since the wind velocities for adjacent heights in the wind profiles are highly correlated, most of the variance in the data is retained by a limited number of principal components. The percentage of variance retained is calculated by the sum of the eigenvalues of the retained principal components divided by the sum of the eigenvalues of all components. In Fig. 3 it can be observed that for the first four principal components more than 90 % of the variance is retained for the MMIJ DOWA dataset. The wind profile shape data mapped to the space spanned by its first five principal components is used as input for the clustering.

Figure 4a shows the frequency distribution of the wind profile shapes in the PC1, PC2-space. Note that the mean of the dataset in the principal component space coincides with the origin. The PC1, PC2-projection of the wind profile shapes in the

https://doi.org/10.5194/wes-2019-108
Preprint. Discussion started: 17 January 2020

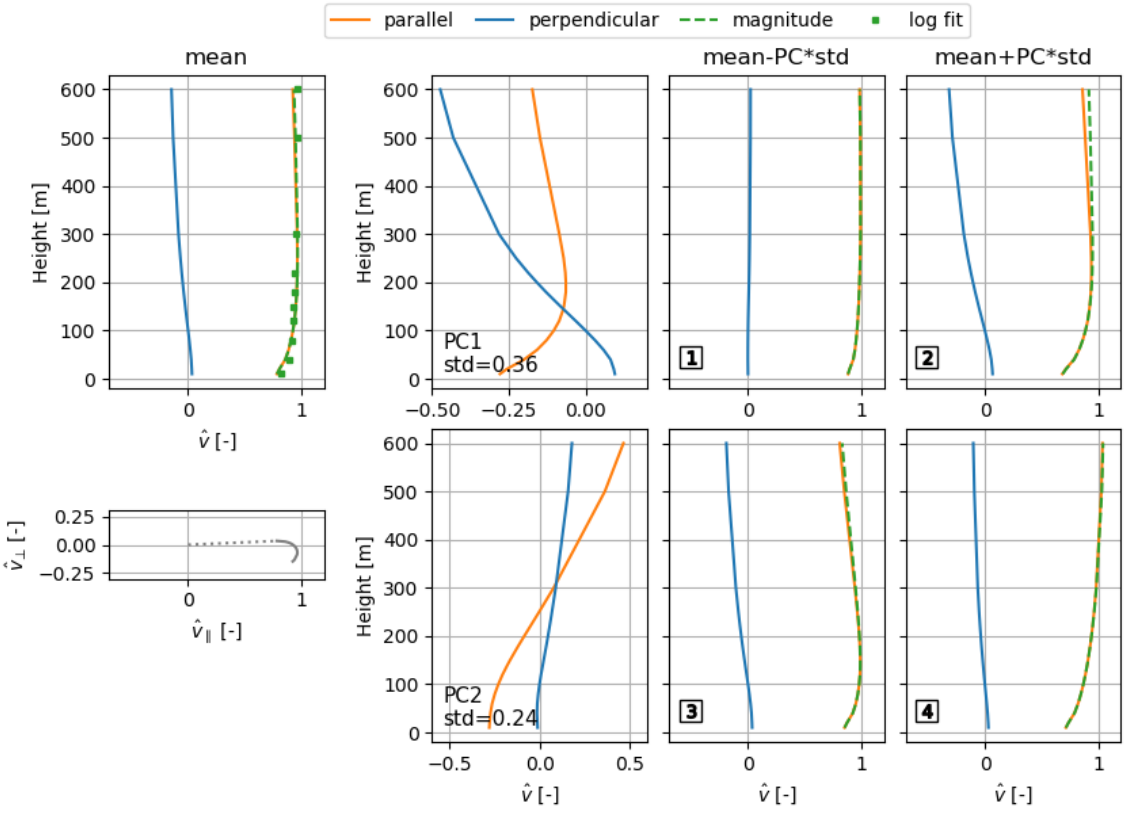

Figure 2. MMIJ DOWA data: Mean vertical wind profile shape (top-left) and corresponding top-view/hodograph (bottom-left), the first and second principal components (2nd column), and wind profile shapes along the principal components axes (3rd and 4th column). Plus and minus one standard deviation is also plotted for the first two PCAs.

3rd and 4th column of Fig. 2 are indicated with the markers. At first glance, two clusters can be observed: a confined cluster with a high concentration of data points with its center roughly at (-0.35, 0.0) and a more spread out cluster which resembles a tail extending from the first cluster with its centroid roughly at (0.25, 0.25). No other distinct clusters were observed by visually inspecting the projections of combinations of the first five PCs. Figure 4b will be discussed in Sect. 4.2.

3.3 Number of clusters

K-means clustering is used to identify clusters in the dataset (Pedregosa et al., 2011). In k-means clustering, each cluster is represented by a centroid and each sample is assigned to its nearest cluster centroid. The clustering algorithm iteratively attempts to find (the positions of) the cluster centroids that minimise the sum of the Euclidean distances of all samples to their nearest centroid, using the Within-Cluster Sum of Squares (WCSS) as a cost function. K-means clustering is always able to produce a result, which makes it very powerful but also potentially deceptive. The algorithm has some limitations as it is sensitive to outliers and noise and has the tendency to produce spherical clusters of equal magnitude. Moreover, the result is

https://doi.org/10.5194/wes-2019-108
Preprint. Discussion started: 17 January 2020

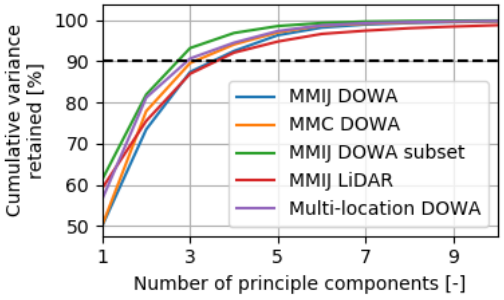

Figure 3. Relationship between the percentage of variance retained and the number of principal components for all the analysed datasets.

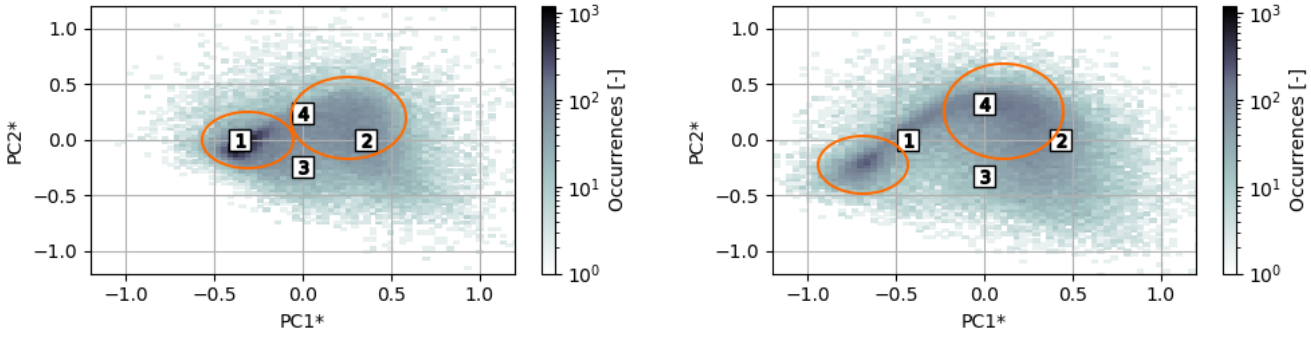

(a) MMIJ (b) MMC

Figure 4. Sample frequency distributions in the PC1, PC2-space using the DOWA data. The mean normalised wind profile shape coincides with the origin, the markers show the PC1, PC2 projection of the wind profile shapes in the 3rd and 4th column of Fig. 2 and 10, for MMIJ and MMC respectively.

highly sensitive to the choice of itk (the number of clusters) and it is often not evident how many clusters to use. The elbow and silhouette method are used for finding an appropriate number for itk.

The elbow method investigates the trend of the number of clusters as a function of the WCSS. Increasing the number of clusters is equivalent to reducing the WCSS. Kinks in the trend should be indicators of appropriate choices for itk. The elbow plot in the upper panel of Fig. 5a does not show any distinct kinks for more than three clusters. Although not shown here, the cluster model is not prone to over-fitting for the evaluated range of the number of clusters.

The silhouette score, ranging from -1 to 1, expresses the similarity of a sample to the other samples in its cluster with respect to the similarity of that sample to the closest neighbouring cluster's samples. The middle panel of Fig. 5a shows the number of clusters against the mean silhouette score. The highest mean silhouette score is found for two clusters and the overall trend is a decreasing mean silhouette score for an increase in the number of clusters.

https://doi.org/10.5194/wes-2019-108
Preprint. Discussion started: 17 January 2020

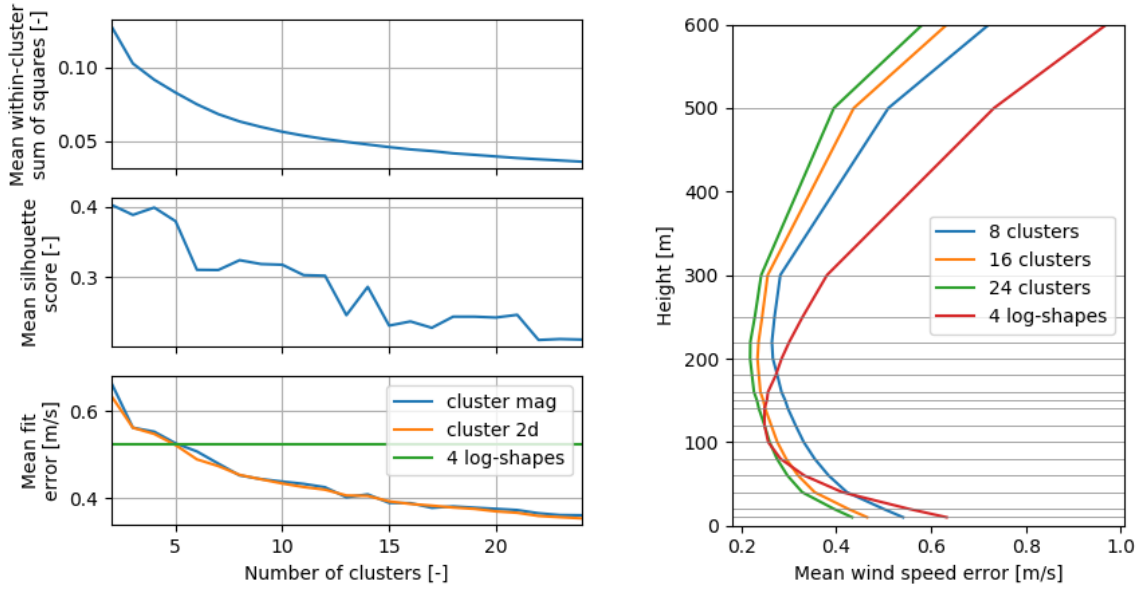

(a) The cost function of the clustering algorithm (top), the silhouette score metric for the cohesiveness of the clusters (middle), and the wind speed equivalent of the cost function (bottom).

(b) Mean wind speed (magnitude) error with height for a logarithmic profile (using a roughness length of 0.0002 m and four stability conditions) and three cluster representations.

Figure 5. Clustering performance relative to the number of clusters.

In agreement with visual inspection of Fig. 4a, the silhouette score trends shows that using two clusters is favourable. However, to get a sensible representation of the wind resource for AEP estimation, more clusters are desirable. This will be discussed in Sect. 5.2. The number of clusters should at least yield a more accurate wind resource representation than when using only logarithmic wind profiles. The accuracy of the representation is assessed by the mean fit error of the filtered samples in the wind profile data (mean wind speed greater than 5 $\mathrm{m\,s^{-1}}$, before normalisation). Next, it is discussed how a sample's fit error is calculated for the logarithmic profile and cluster representation.

For each sample categorised within a cluster the wind profile is generated using the cluster's representative wind profile shape multiplied by the normalisation wind speed. The error is expressed as the root mean square of the wind speed errors of profile predicted minus actual wind speed for both the parallel and perpendicular components at each height. The 'cluster 2d'-line in the lower panel of Fig. 5a shows the relationship between the fit error and the number of clusters when looking at the parallel and perpendicular components individually. Note that the cost function in the k-means clustering is quadratically proportional to the mean fit error of the cluster representation. The same calculated error but only using the magnitude of the wind speed is shown by the 'cluster mag'-line. The lines show that both error metrics give virtually the same result.

A comparison is made against using a series of logarithmic profile fits using least squares fitting. Logarithmic profiles with a roughness length of 0.0002 m are fitted to each sample using the wind speed at 100 m for four Obukhov lengths ranging from very unstable to near neutral stable conditions: -100, -350, 10^{10}, and 350 m and neglecting wind direction dependence. The

https://doi.org/10.5194/wes-2019-108
Preprint. Discussion started: 17 January 2020

eawe european academy of wind energy
Open Access WIND ENERGY SCIENCE DISCUSSIONS

best fit of every sample is used to calculate the average fit error of the dataset. The lower panel of Fig. 5a shows that the cluster profile representation yields a smaller error than the logarithmic profile representation when using just three clusters or more.

The error of the resulting fits as a function of height are assessed using Fig. 5b. The horizontal grid lines indicate the 17 heights at which the wind speeds are provided in the DOWA dataset. For each individual height, the mean wind speed error is plotted. Around 150 m height, the grid is relatively fine, which is equivalent to the least squares fitting having a higher weight in this region. This results in the fits having a relatively low mean wind speed error around 150 m and a relatively high error at 10 m and 600 m. Although the accuracy at 100 m of the cluster representation using eight clusters is lower than that of the logarithmic profile representation, the overall mean error is substantially lower.

For the remainder of this paper, eight clusters are used, following a trade-off between the mean wind profile fit error, the silhouette score, and not having an excessive number of profiles.

To get more insight in the structures of the individual clusters, the mean silhouette score of their samples is calculated. Figure 6 shows that cluster 1–4 have a relatively large number of samples with high silhouette scores and thus are cohesive clusters. The silhouette score distributions of clusters 5–8 indicate a less uniform set of samples, especially that of cluster 8. The higher the mean silhouette score, the more likely it is that a cluster is representing a natural structure in the data. The physical interpretation of the clusters is further discussed in the next section.

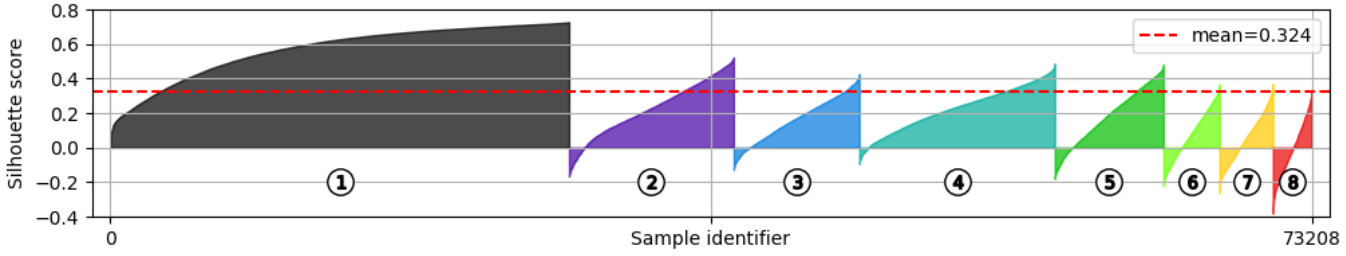

Cluster label	MMIJ-1	MMIJ-2	MMIJ-3	MMIJ-4	MMIJ-5	MMIJ-6	MMIJ-7	MMIJ-8	overall
Mean silhouette score	0.567	0.226	0.164	0.226	0.184	0.080	0.056	-0.009	0.324

Figure 6. The silhouette scores of the individual samples grouped by cluster and in ascending order for MMIJ DOWA. The colour indicates to which cluster the sample belongs to. The overall mean score is indicated by the dashed line and the table below the figure states the mean score for each cluster.

https://doi.org/10.5194/wes-2019-108
Preprint. Discussion started: 17 January 2020

eawe european academy of wind energy
Open Access WIND ENERGY SCIENCE DISCUSSIONS

4 Wind resource representation based on clusters

Firstly, the results of the clustering procedure for the MMIJ location using the DOWA dataset are presented and each cluster is investigated by studying patterns in its occurrence and its affinity with other characteristics. Secondly, the analysis is repeated for the MMC location. The results are used to shed light on the spatial variability of profile clusters. This provides confidence that the methodology is suitable for various individual sites. Next, LiDAR observations at the MMIJ location are used for the clustering. The resulting wind profile shapes are compared to those obtained from the DOWA data. It is preferable to have a single set of clusters that is applicable for a wide range of sites. Therefore, lastly, clusters are obtained using DOWA data from 45 locations. The resulting clusters are used to make maps of the wind resource for the DOWA domain.

4.1 Interpretation of prevailing wind profile shapes at MMIJ

The representative wind profile shapes for the eight clusters are presented in Fig. 8. Logarithmic profiles with a roughness length of 0.0002 m are fitted to the resulting shapes. The shapes of wind profiles 1–3 resemble that of logarithmic profiles albeit with different rates of wind shear. Both wind shear and veer increase moving between shapes 1 to 3. The fitted Obukhov lengths correspond to very unstable and neutral stability conditions, respectively (-8, 7500, and 800 m).

The veering of the profiles can be clearly observed in the top-view plots of the wind profile shapes. Cluster 4–7 all exhibit wind speed maxima roughly between 100 and 200 m, indicating potential low-level jets. Cluster 8 also resembles a neutral logarithmic profile, however, the wind direction is unusual in that the perpendicular wind speed component initially decreases with height below 120 m but then increases sharply above this height. It should be noted that as this corresponds to an incohesive cluster, one could expect that the shape gives a poor representation of the cluster samples. As will be shown later, this wind profile shape occurs mostly at low wind speeds. Possibly, the kink at 120 m coincides with a physical feature such as the top of an (internal) boundary layer, or with the reversal height of the sea breeze circulation but this would need further investigation.

In Fig. 7a, it is seen that the cluster centroids are well spread over the PC1, PC2-space, though clusters 5 and 7 show significant overlap. However, this figure only shows two axes of the five-dimensional space. If the five PC coordinates of the cluster centroids are examined in Table 1, it can be seen that clusters 5 and 7 differ significantly along the PC3 dimension. From Table 1, it can be deduced that for distinguishing between the eight profile clusters it is sufficient to use the first three PCs.

From the breakdown of cluster frequencies in the filtered and full datasets shown in Table 2, it can be seen that cluster 1 dominates in the MMIJ filtered dataset with a frequency greater than 38 %.

After the cluster mapping is obtained using the filtered data, it is used to also assign the calm wind samples to one of the clusters. It can be seen that the frequency distribution of the filtered and full datasets do not differ significantly. This suggests that the filtered dataset is a good representation of the full dataset.

To further investigate the cluster characteristics, cluster frequency distributions are broken down as a function of various time periods, wind speed range, wind direction and atmospheric stability. The resulting frequency distributions are shown in Fig. 9. The bin limits are chosen such that the overall frequency is roughly equal for each bin (except for the wind direction

https://doi.org/10.5194/wes-2019-108
Preprint. Discussion started: 17 January 2020

eawe european academy of wind energy
Open Access WIND ENERGY SCIENCE DISCUSSIONS

bins, which are of equal range). The atmospheric stability metric used for Fig. 9f is the bulk Richardson number:

$$\mathrm{Ri_B} = \frac{\frac{\mathrm{g}}{\bar{\theta}_\nu}\frac{\Delta\theta_\nu}{\Delta \mathrm{z}_\theta}}{\left(\frac{\Delta \mathrm{u}}{\Delta \mathrm{z_u}}\right)^2 + \left(\frac{\Delta \mathrm{v}}{\Delta \mathrm{z_v}}\right)^2} \tag{2}$$

in which g is the gravitational acceleration, $\bar{\theta}_\nu$ is the mean virtual potential temperature, and $\Delta\theta_\nu$, Δu, and Δv are the virtual potential temperature and horizontal wind component differences across the corresponding layers with thicknesses Δz_θ, Δz_u, and Δz_v. The 2 m temperature, skin temperature, and the easterly and northerly components of the 10 m wind velocity from ERA5 surface data are used to approximate the bulk Richardson number (Kalverla et al., 2019). The absolute temperature is used due to the small height difference between the skin temperature and the air temperature and the relatively small effect of humidity. Positive values indicate stable stratification, negative values indicate unstable stratification, and small absolute values correspond to near-neutral conditions.

Cluster label	PC1	PC2	PC3	PC4	PC5
MMIJ-1	-0.33	-0.05	-0.04	-0.02	0.01
MMIJ-2	0	0.17	-0.08	0.05	0.02
MMIJ-3	0.38	0.38	-0.01	0.05	0
MMIJ-4	0.35	-0.02	0.04	-0.09	-0.06
MMIJ-5	0	-0.22	-0.16	0.07	-0.04
MMIJ-6	0.74	-0.4	0.02	0	0.12
MMIJ-7	0.14	-0.33	0.44	0.09	0.03
MMIJ-8	-0.36	0.36	0.45	0.04	0.02

Table 1. Principal component coordinates of cluster centroids for MMIJ DOWA.

https://doi.org/10.5194/wes-2019-108
Preprint. Discussion started: 17 January 2020

eawe european academy of wind energy
Open Access WIND ENERGY SCIENCE DISCUSSIONS

		Cluster number							
dataset	Fraction of full	1	2	3	4	5	6	7	8
Filtered MMIJ DOWA	83.5 %	38.2 %	13.7 %	10.5 %	16.3 %	9.0 %	4.7 %	4.4 %	3.2 %
Full MMIJ DOWA	-	35.8 %	12.2 %	10.6 %	14.0 %	8.8 %	6.5 %	6.5 %	5.7 %
Filtered MMC DOWA	75.0 %	16.2 %	13.8 %	20.6 %	16.3 %	15.6 %	8.2 %	5.4 %	3.8 %
Full MMC DOWA	-	18.4 %	11.8 %	17.1 %	14.1 %	13.4 %	10.1 %	8.3 %	6.8 %
Filtered multi-location DOWA	78.1 %	21.5 %	14.4 %	6.2 %	13.6 %	14.3 %	6.3 %	14.5 %	9.2 %
Full multi-location DOWA	-	20.9 %	12.5 %	8.3 %	14.4 %	13.7 %	8.1 %	13.2 %	9.0 %

Table 2. The fraction of samples assigned to each cluster in both the full and filtered dataset for MMIJ DOWA. The filtered dataset only contains samples that have a mean wind speed greater than 5 $\mathrm{m\,s^{-1}}$.

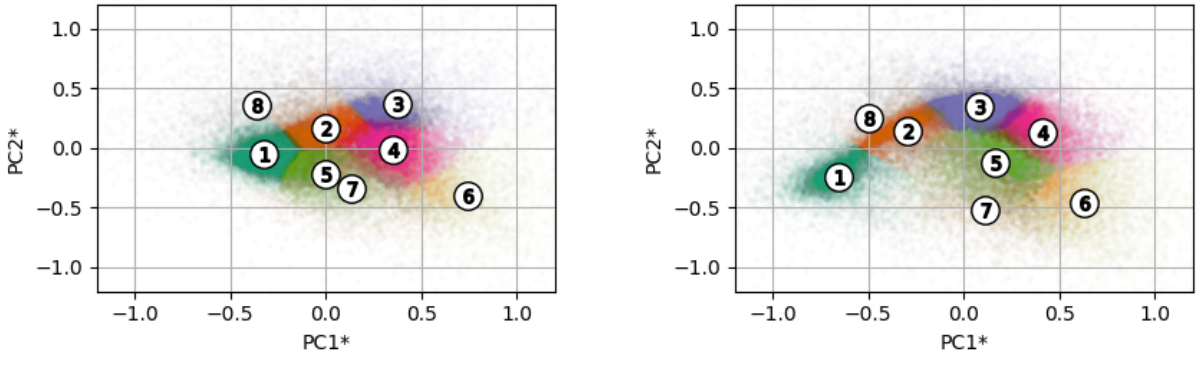

(a) MMIJ (b) MMC

Figure 7. Projection of the samples onto the PC1, PC2-space for the DOWA dataset. The colour indicates to which cluster a sample belongs and the markers represent the clusters centroids.

https://doi.org/10.5194/wes-2019-108
Preprint. Discussion started: 17 January 2020

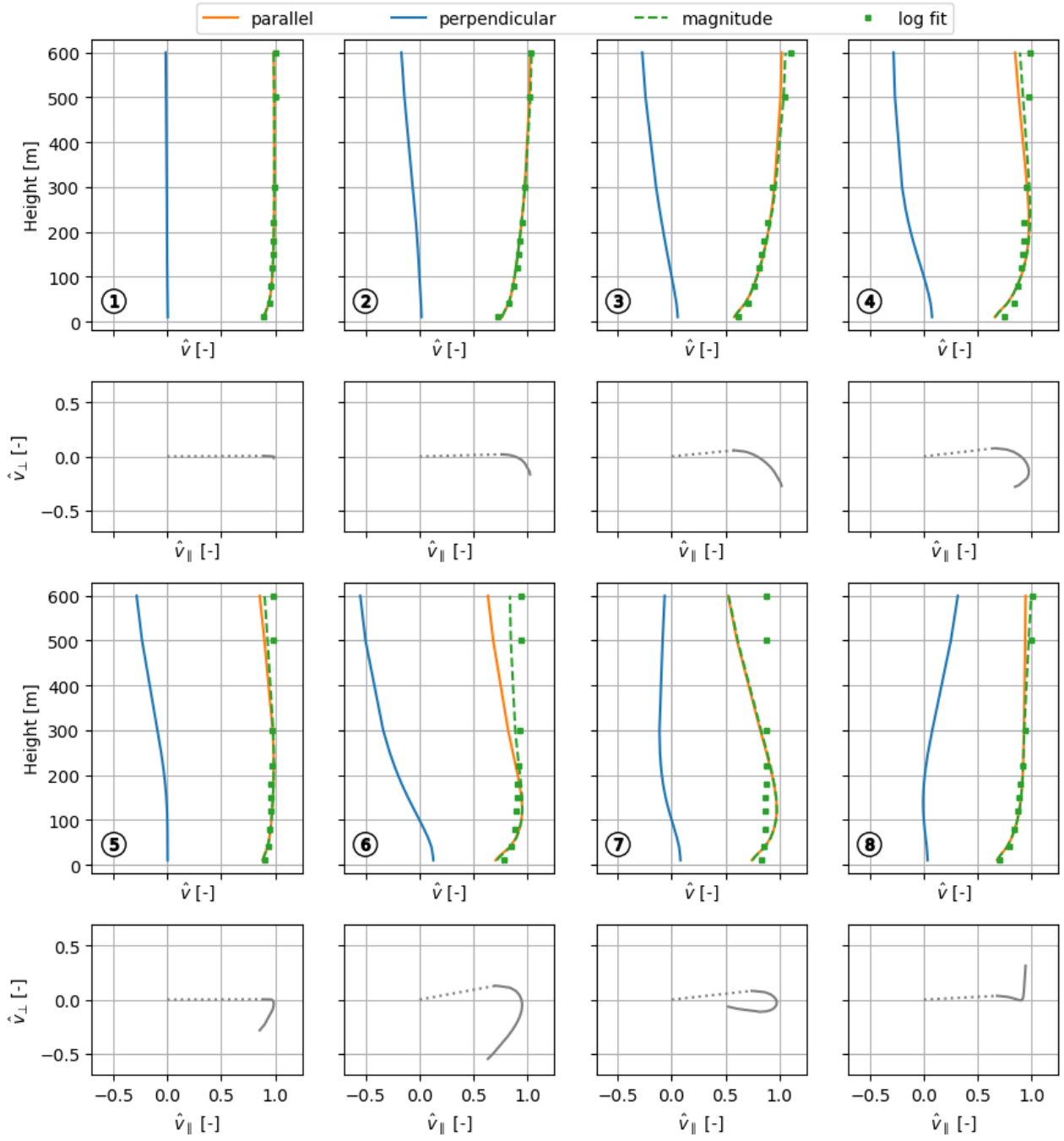

Figure 8. A comparison of the eight profile shapes determined using the clustering procedure for MMIJ DOWA: vertical wind profile shapes (1st and 3rd row) and corresponding top-views/hodographs (2nd and 4th row).

https://doi.org/10.5194/wes-2019-108
Preprint. Discussion started: 17 January 2020

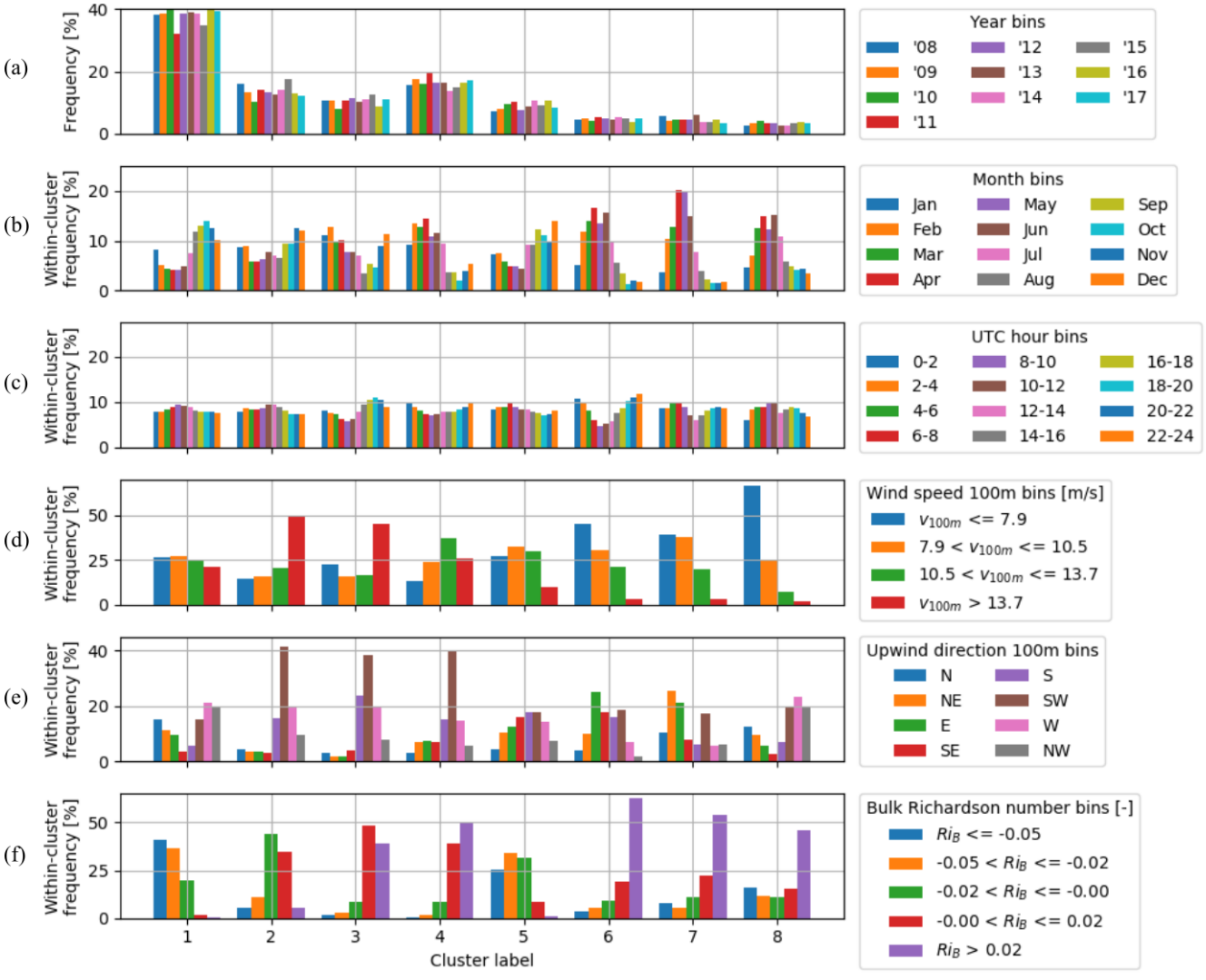

Figure 9. Frequency distributions broken down by time, wind speed range, wind direction and atmospheric stability for MMIJ DOWA. The bins have the same overall frequency, except for the wind direction bins, which are of equal range.

https://doi.org/10.5194/wes-2019-108
Preprint. Discussion started: 17 January 2020

eawe european academy of wind energy
Open Access WIND ENERGY SCIENCE DISCUSSIONS

The upper panel shows that there is only a small amount of inter-annual variability in the clusters and no clear cycles over the 10 years analysed. This is a prerequisite for using the cluster representation for the AEP calculation for wind energy systems. We will now discuss the characteristics of each cluster based on Figs. 7a, 8, and 9b–f.

Cluster 1 occurs predominantly in the autumn (Fig. 9b) and is slightly more frequent in the morning hours. Wind speeds are weak or moderate, but not so frequently strong. Winds are more frequently from the W, NW or N directions. The Richardson number is typically negative suggesting predominantly unstable conditions. These characteristics help to explain the profile shape for cluster 1. In autumn, the relatively warm sea water favours neutral to unstable stratification; the W, NW and N directions have long fetches over sea which ensures that the boundary-layer has had enough time to establish an equilibrium profile. In unstable conditions, the wind profile is typically will mixed, resulting in a rather homogeneous wind profile showing little veer with height, consistent with the cluster 1 profile shape in Fig. 8.

If we now look at clusters 2 and 3, we see that both these clusters are typically found for strong winds, predominantly from the south-west. Strong south-westerly winds are characteristic for the wind climate at this mid-latitude location, which is dominated by the frequent passage of low-pressure systems. The Richardson number is highest for cluster 3, though cluster 2 also shows a tendency for stable conditions. The stable stratification suppresses turbulent mixing, which helps to sustain a strong wind shear, consistent with the increasing wind shear and veer seen in Figs. 7a and 8. We see that cluster 2 occurs more often in the winter and cluster 3 in the spring, when the sea water is relatively cold – which is favourable for the formation of stable stratification.

Cluster 4 tends to be associated with south-westerly winds and stable stratification. The seasonal cycle is even more pronounced, consistent with the stable stratification in spring. However, wind speeds for cluster 4 are moderate rather than strong. Consequently, the wind profile takes on a slightly jet-shaped form. Low-level jets at MMIJ originating from the south-west may be associated with the mechanism described by Capon (2003): the steep coastlines at either side of the Strait form an orographic ‘gap’ in the lower boundary layer. Under stably stratified conditions, the low-level wind is forced through this opening, leading to an acceleration at the lower levels.

Clusters 5, 6, and 7 also take on jet-shaped wind profiles, but they occur for different conditions. Notably, cluster 5 seems to occur for unstable conditions in autumn. Inspection of Fig. 8 shows that the cluster 5 profile has a weaker jet-like shape and there seems to be a rather abrupt kink, indicative of a discontinuity such as an (internal) boundary-layer top.

Clusters 6 and 7 occur almost exclusively for very stable conditions in spring, but for weak wind situations (as opposed to cluster 4). The wind direction for cluster 6 is not very clearly defined, although a peak is observed for easterly winds. For cluster 7, this peak is more pronounced. Both clusters also have a clear diurnal cycle, with fewer jets around noon. Indeed, various studies have linked low-level jets to the diurnal variation of both the land-sea temperature difference and the intensity of turbulent mixing (e.g., Burk and Thompson, 1996; Parish, 2000; Mahrt et al., 2014; Shapiro et al., 2016). Thus, the low-level jets in clusters 6 and 7 seem to be caused by different mechanisms than those in clusters 4 and 5.

Cluster 8, finally, is also characterised by a distinct kink in the wind profile. The difference with cluster 5 is that this profile occurs in spring, under stable conditions, for different wind directions and more often for winds with a westerly rather than

https://doi.org/10.5194/wes-2019-108
Preprint. Discussion started: 17 January 2020

a southerly component. Possibly, these profiles are caused by the offshore advection of boundary layers (Dörenkämper et al., 2015). In that case, it makes sense that the characteristics of the advected structures influence the wind profile.

4.2 Comparison with an onshore location

The analysis is repeated for the onshore location MMC using the DOWA wind dataset. The mean wind profile shape for MMC is shown in the upper left panel of Fig. 10. The vertical, normalised wind speed (magnitude) profile roughly resembles that of a logarithmic profile, but with a higher wind shear than for MMIJ due to the higher surface roughness. The hodograph of the mean wind profile shape shows that also the wind veer is substantially increased. A logarithmic profile with a roughness length of 0.1 m is fitted to the vertical, normalised wind speed (magnitude). The mean shape shows a good fit with a neutral logarithmic profile.

Figure 10 also shows the first two PC profiles for MMC. Note that the PC1 and PC2 profiles are similar for the MMIJ and MMC locations. The same coordinate system is used for Fig. 4a and b, for which the average PC1 and PC2 profiles of the two locations (denoted using an asterisk) are used as directions for the x-axis and y-axis, respectively. The distribution in Fig. 4b shows a similar pattern to Fig. 4a: a cluster of data points at the left of the figure with a tail of data points extending from the cluster at around 45 degrees. Overall the data points for MMC are more spread out than for MMIJ, particularly along the PC1 axis. Figure 7 shows that for both locations, the confined cluster of data points is cluster 1, which for MMC is less pronounced than for MMIJ. The remaining clusters with logarithmic like wind profile shapes account for most of the tail, which are clusters 2 and 3 for MMIJ and clusters 2–4 for MMC, see Fig. 11. Logarithmic profiles with a roughness length of 0.1 m are fitted to the resulting shapes. The fitted Obukhov lengths of wind profiles 1–4 range from unstable to neutral stability conditions, respectively (-180, 2215, 755, and 925 m). Surprisingly, the Obukhov length that is found for profile 4 is more neutral than that for profile 3. The wind profile shapes for clusters 5–7 show low-level jet features similar to MMIJ. Cluster 8 also exhibits the kink in the vertical wind veer profile.

From Table 2 it can be concluded that cluster 3 is dominant in the MMC filtered dataset with a frequency of 20 %. The frequencies for cluster 1–5 are however similar in contrast to the cluster frequency distribution for MMIJ, which just has one distinct dominant cluster. As for MMIJ, clusters 6–8 are the least dominant. From Fig. 12, a distinction can be made between winter and spring clusters, namely clusters 2–6 and clusters 1, 7, and 8, respectively. The diurnal cycles are highly pronounced in contrast to those of MMIJ. This makes sense, because the land surface, as opposed to the sea surface, has a relatively lower heat capacity and promoting more immediate heat transfer to or from the atmosphere. Thus, in the presence of daytime solar irradiation, convection is created, and well-mixed profiles are expected, whereas at night, stable stratification is more frequent. Clusters 1 and 2 predominantly occur during the day and clusters 3–8 during the night. Note that low-level jets (and stable conditions in general) occur almost exclusively at night. The diurnal cycle over land is comparable to the seasonal cycle over sea. Stable conditions occur in spring for MMIJ, and at night for MMC. Note that the wind speed and Richardson number bin limits are different for MMC and MMIJ to ensure that the overall frequency is equal for each bin. Nevertheless, the wind speed frequency distribution over the bins is almost identical to that for MMIJ. Also the wind direction frequency distribution

https://doi.org/10.5194/wes-2019-108
Preprint. Discussion started: 17 January 2020

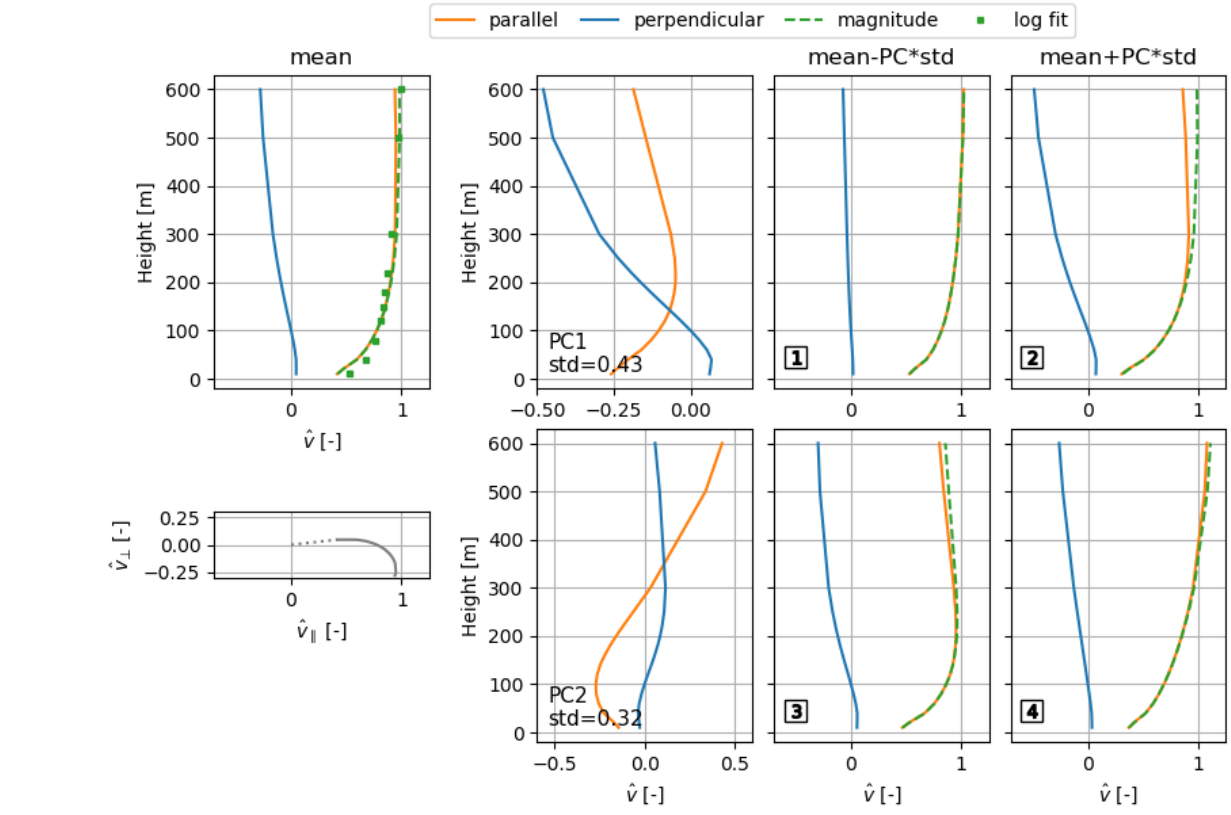

Figure 10. MMC DOWA dataset: mean vertical wind profile shape (top-left) and corresponding top-view/hodograph (bottom-left), the first and second principal components (2nd column), and wind profile shapes along the principal components axes (3rd and 4th column).

https://doi.org/10.5194/wes-2019-108
Preprint. Discussion started: 17 January 2020

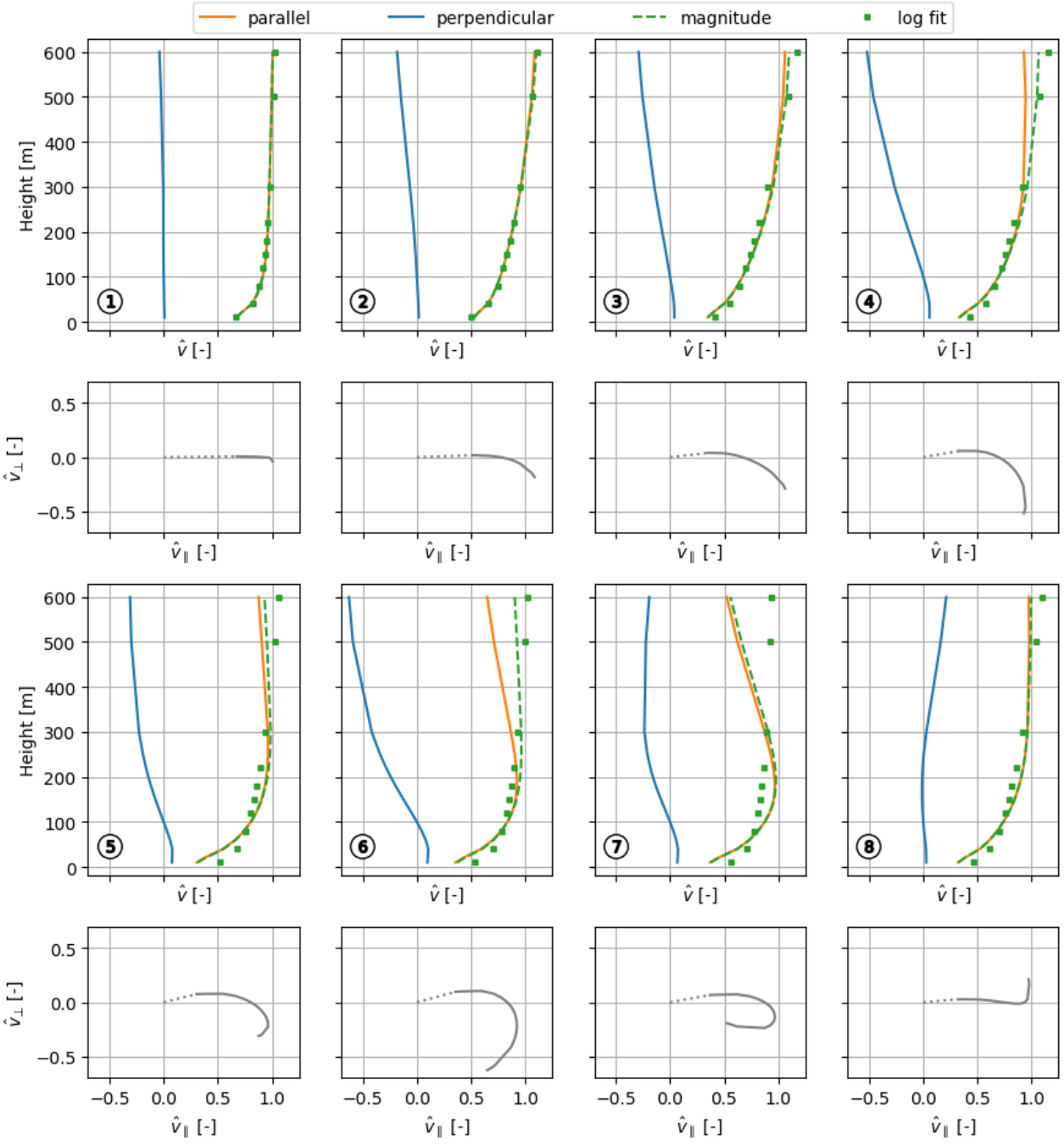

Figure 11. A comparison of the eight profile shapes determined using the clustering procedure for MMC DOWA: vertical wind profile shapes (1st and 3rd row) and corresponding top-views/hodographs (2nd and 4th row).

https://doi.org/10.5194/wes-2019-108
Preprint. Discussion started: 17 January 2020

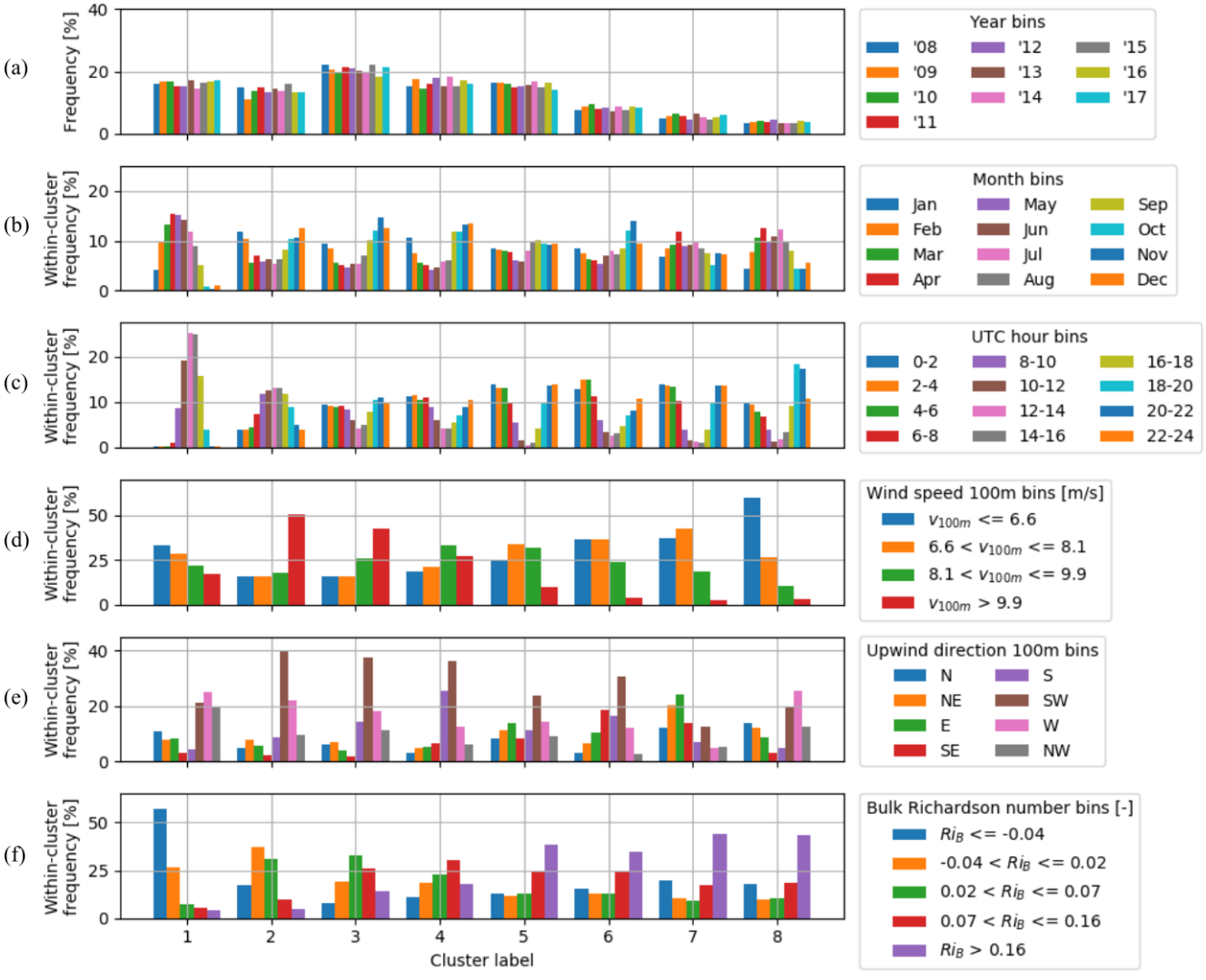

Figure 12. Frequency distributions broken down by time, wind speed range, wind direction and atmospheric stability for MMC DOWA. The bins have the same overall frequency, except for the wind direction bins, which have equal ranges.

https://doi.org/10.5194/wes-2019-108
Preprint. Discussion started: 17 January 2020

eawe european academy of wind energy
Open Access WIND ENERGY SCIENCE DISCUSSIONS

4.3 Validation with LiDAR observations

In order to investigate that the DOWA data and the LiDAR observations give similar cluster profile shapes, we present the clustering results that follow from the MMIJ LiDAR observations. The cluster profiles shapes obtained using the hourly-averaged LiDAR observations are shown as solid lines in Fig. 13. Linear interpolation is used to obtain the wind velocities for the equivalent heights to the LiDAR measurements from the DOWA dataset. Clustering is repeated for the interpolated data, to compare the clusters for the LiDAR observations and the DOWA dataset. The cluster profiles using the DOWA interpolated data are shown as dashed lines in Fig. 13 for comparison. It can be seen that the cluster profile shapes for both datasets are very similar. Similar results are observed using the 10-minute averaged LiDAR observations (not shown).

4.4 Spatial distribution of wind profile shapes

In this section, the clustering procedure is performed using DOWA data at 45 grid points over a large area marked on the map in Fig. 1. These are selected such that onshore, coastal, and offshore locations are equally represented in the sample set.

Figure 14 shows the wind profile shapes for the multiple location (ML) clusters. The cluster mapping is obtained using the filtered data of the 45 locations. Subsequently, the cluster mapping is applied to the data of all the grid points in the DOWA dataset to determine the cluster frequency distribution at every grid point.

For each cluster, a map is generated showing the spatial distribution of its frequency of occurrence, see Fig. 15. Clear patterns can be be observed in the area for which a cluster is more frequently occurring. The maps show a distinct division between clusters that mostly occur over sea (clusters 1–3) and over land. The over land clusters are further sub-divided into coastal and onshore clusters, see Table 3. Since cluster 1 is dominant around the MMIJ location, a similar cluster is expected based on the set of clusters determined earlier using this single location. Comparing Figs. 8 and 14 indeed shows a good match between the wind profile shape for cluster 1 determined using the multiple cluster analysis (ML-1) and that determined using the single location analysis (MMIJ-1), which was previously identified as the dominant cluster. The frequency of cluster ML-7 is highest for the MMC location, see Table 3. The corresponding wind profile shape shows a strong resemblance with those associated with the dominant clusters determined using the single site analysis of MMC (*i.e.* MMC-3 and MMC-4). Despite the fact that cluster ML 7 is most frequent in hilly areas, it is still dominant for the flat MMC location. Every ML-cluster is matched to a single location clusters based on visual resemblance of their wind profile shapes, see Table 3.

https://doi.org/10.5194/wes-2019-108
Preprint. Discussion started: 17 January 2020

eawe european academy of wind energy
Open Access WIND ENERGY SCIENCE DISCUSSIONS

Cluster label	Class	Most frequent area	Matching single location cluster(s)	MMIJ frequency	MMC frequency
ML-1	offshore	far offshore	MMIJ-1	48.5 %	5.8 %
ML-2	offshore	near offshore	MMIJ-2, 3	22.0 %	4.2 %
ML-3	offshore	English Channel	MMIJ-4, 6	14.1 %	4.2 %
ML-4	coastal	coast	MMC-1	8.6 %	16.1 %
ML-5	onshore/coastal	rapid increase in elevation	MMC-2	3.0 %	17.4 %
ML-6	onshore	valleys	MMC-6	2.0 %	13.3 %
ML-7	onshore	hills	MMC-3, 4	1.2 %	21.7 %
ML-8	onshore	flat land	MMC-5	0.6 %	17.3 %

Table 3. Classification of the multiple location clusters from the DOWA data.

https://doi.org/10.5194/wes-2019-108
Preprint. Discussion started: 17 January 2020

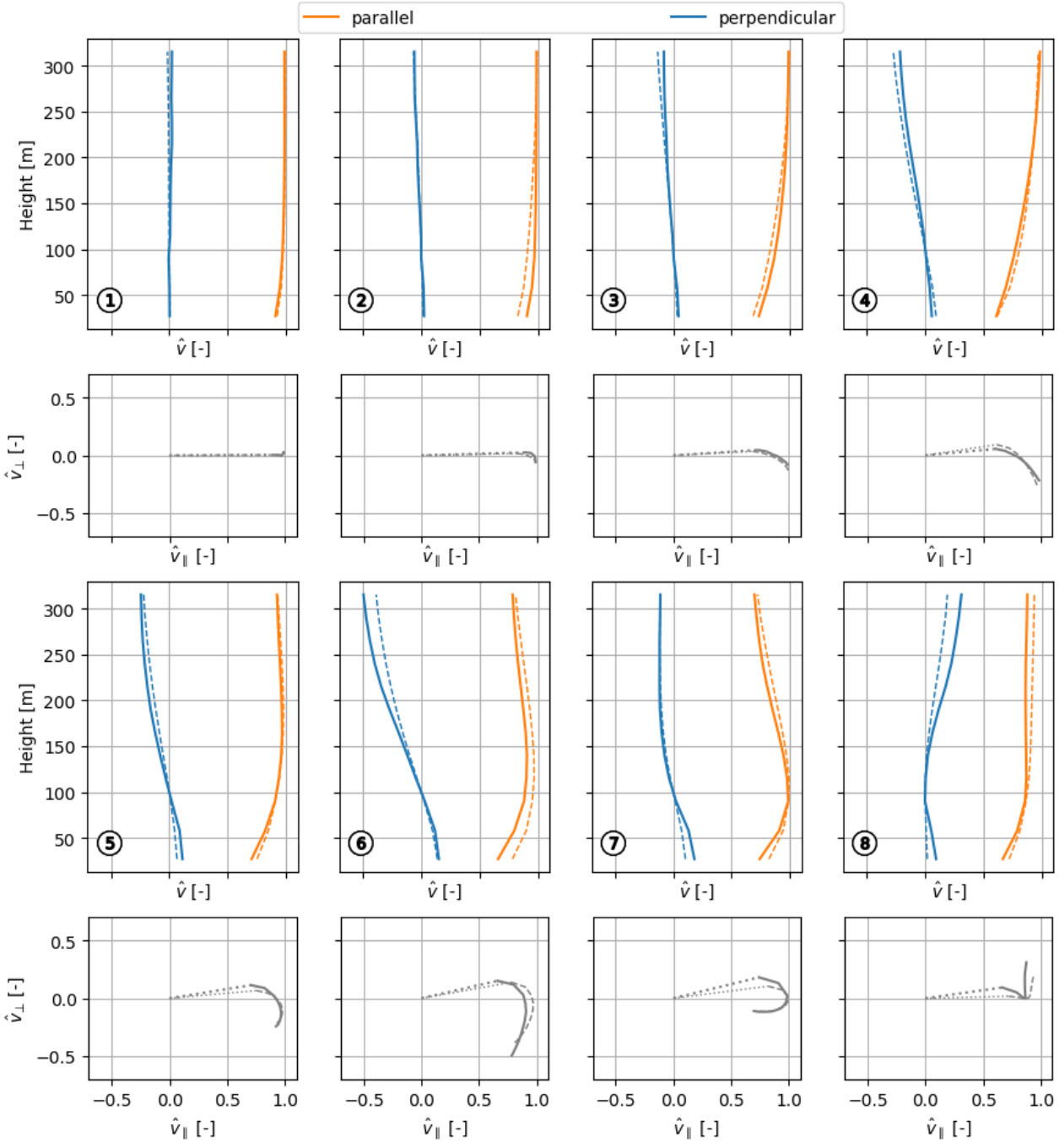

Figure 13. A comparison of the eight profiles shapes determined using the clustering procedure for MMIJ from the LiDAR observations (solid lines) and the interpolated DOWA data (dashed lines): vertical wind profile shapes (1st and 3rd row) and corresponding top-views/hodographs (2nd and 4th row).

https://doi.org/10.5194/wes-2019-108
Preprint. Discussion started: 17 January 2020

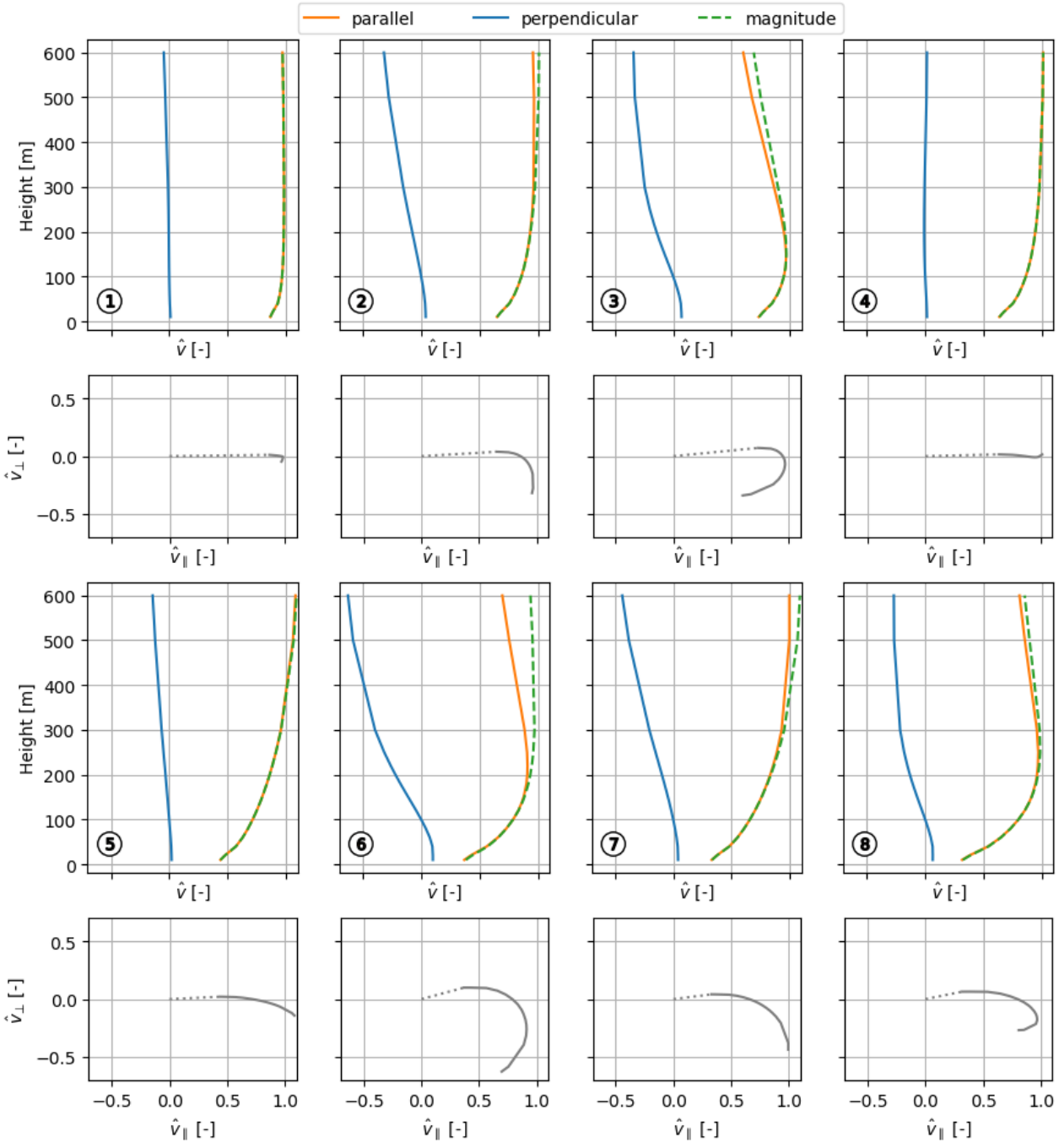

Figure 14. A comparison of the eight profile shapes determined using the clustering procedure based on the data from the 45 locations in Fig. 1: vertical wind profile shapes (1st and 3rd row) and corresponding top-views/hodographs (2nd and 4th row).

https://doi.org/10.5194/wes-2019-108
Preprint. Discussion started: 17 January 2020

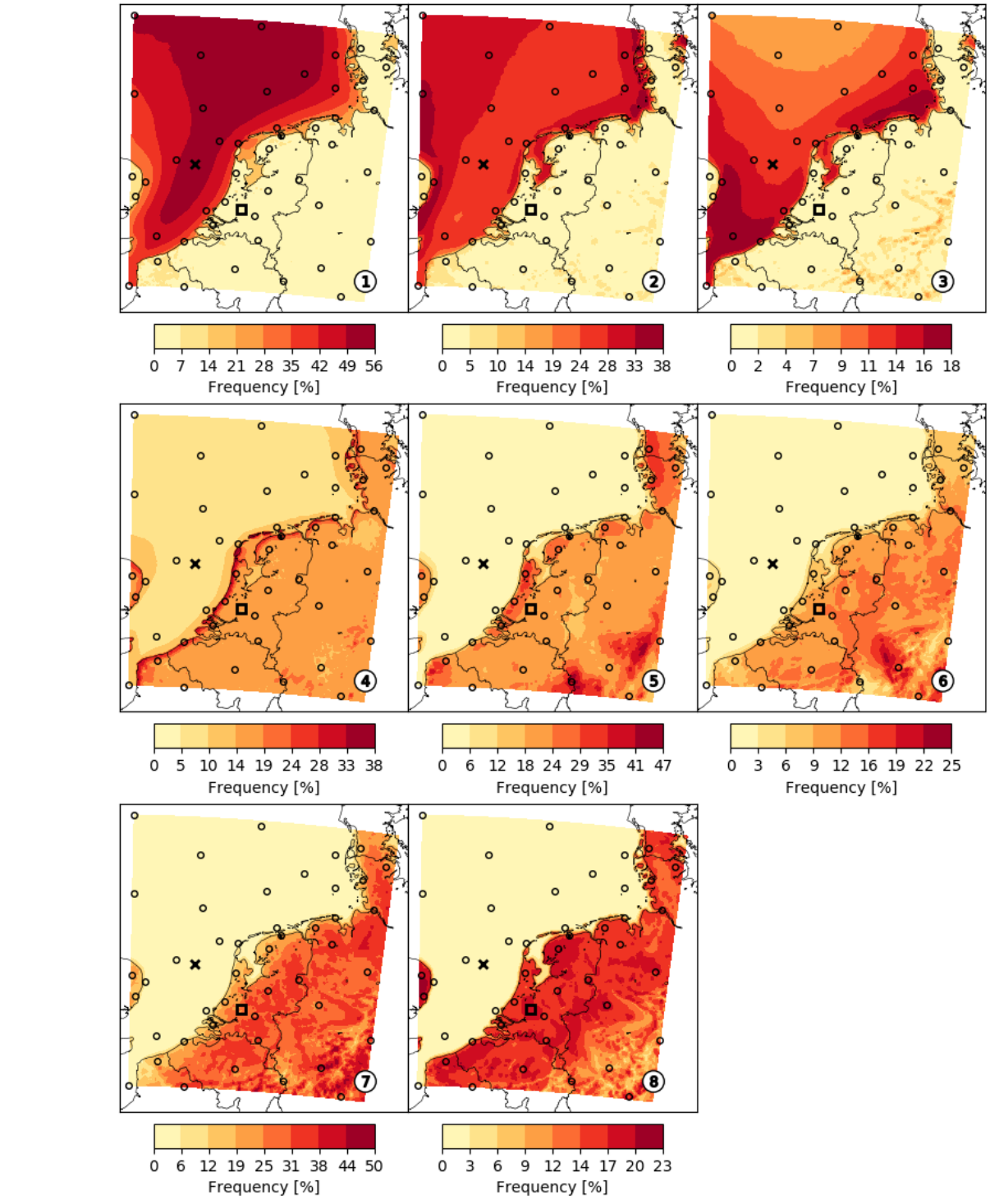

Figure 15. Frequency of occurrence of each multiple location cluster mapped over the DOWA domain.

https://doi.org/10.5194/wes-2019-108
Preprint. Discussion started: 17 January 2020

5 Fast AWE production estimation based on historical wind data

This section demonstrates how the wind profile shapes that are obtained from the clustering procedure can be used for calculating the AEP of a pumping AWE system. The AEP is calculated for the MMC location using the wind profile shapes from Sect. 4.2. For each of these shapes, a power curve is generated for the considered system and its AEP contribution is determined. Finally, the sensitivity of the total AEP to the number of clusters is evaluated.

5.1 Determining power curves for AWE systems operated in pumping mode

A pumping AWE system is alternating between reeling the tether in and out and thereby producing and consuming power, respectively. When reeling out, the kite generates a high lift force that pulls the tether from the drum of the ground station and drives the generator. Following this traction phase, the tether is reeled back in at a fraction of the reel-out power by decreasing the lift force and following an appropriate flight path. The specific operational approach differs per concepts. Flexible-kite systems typically sweep a large height range during the pumping cycle, which requires pronounced transitions between these two working phases. In this work, we only evaluate a flexible-kite system, however, the methodology can in principle be applied to any kind of pumping AWE system.

Figure 16 shows the distinct phases of a pumping flexible-kite system. During the traction phase, the kite flies figure-eight manoeuvres in a fast cross-wind motion. After the traction phase, the cross-wind flight is ended, the kite is depowered, and pointed towards the zenith. Once reeled back in, the kite is steered down and transitions again to the traction phase.

The Quasi-Steady Model (QSM) presented by Van der Vlugt et al. (2019) is used to determine the power output of a pumping AWE system. The model moves the kite along an idealised flight path conform a series of computed steady states, which is a reasonable approximation for a lightweight membrane kite. The idealised flight path is composed of only three phases: the retraction, transition, and traction phase. The transition between the traction and retraction phase is not modelled separately, but is included in the retraction phase. The cross-wind flight manoeuvres during the traction phase are not resolved but represented by an average cross-wind flight state with constant values for the elevation, azimuth, and course angle.

The QSM assumes a steady wind field with a varying wind speed along the height. Because the original implementation of the QSM does not account for changes in wind direction along the height, only the magnitude distributions of the wind profile shapes are used to describe the wind environment. Using these unidirectional wind profile shapes is equivalent to hypothetically knowing the wind direction profile and steering the kite to correct for direction changes. A power curve is constructed for each of the wind profile shapes.

The system properties that are used as model input are given in Table 4. C_L and C_D are the lift and drag coefficient, respectively. These kite properties are based on the leading edge inflatable V3 kite as presented in Oehler and Schmehl (2019).

For each phase of a cycle, either the tether force or the reeling speed is controlled in the simulation. Although the tether force during reel-in is substantially lower than during reel-out, it should be sufficiently high to achieve a fast retraction of the kite. During the transition phase, the reeling speed is kept zero unless tether force limits are exceeded. Lastly, during the traction phase, a set value of the tether force is applied that maximises the mean cycle power.

https://doi.org/10.5194/wes-2019-108
Preprint. Discussion started: 17 January 2020

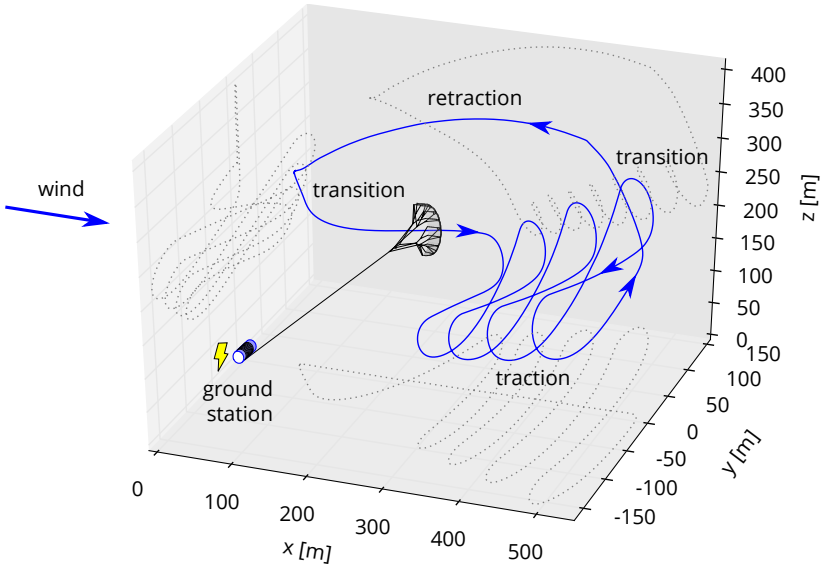

Figure 16. Flight path of the flexible-kite, pumping AWE system (kite & drum not to scale) adapted from Fechner (2016).

Kite properties		Tether properties		Operational limits		Representative reel-out state	
Projected area	19.75 m^2	Density	724 $\mathrm{kg\,m}^{-3}$	Min. reeling speed	2 $\mathrm{m\,s}^{-1}$	Azimuth angle	13°
Mass	22.8 kg	Diameter	4 mm	Max. reeling speed	10 $\mathrm{m\,s}^{-1}$	Course angle	100°
$C_{L,\mathrm{powered}}$	0.9	$C_{D,\mathrm{tether}}$	1.1	Min. tether force	300 N		
$C_{D,\mathrm{powered}}$	0.2			Max. tether force	5000 N		
$C_{L,\mathrm{depowered}}$	0.2						
$C_{D,\mathrm{depowered}}$	0.1						

Table 4. Constant system properties that are used as model input for the QSM.

Numerical optimisations are used to determine the control strategy that maximises the mean cycle power by varying the parameters that are listed in Table 5. For high wind speeds, the system is expected to run into its limits such as the maximum tether force. One option for lowering the tether force is increasing the elevation angle of the kite. The effective pumping length of the tether is varied while maintaining a minimum tether length of 200 m.

The optimisations are performed using the sequential quadratic programming algorithm (SLSQP) that is part of pyOpt (Perez et al., 2012). This class of algorithms is generally seen as a good general-purpose method for differentiable constrained non-linear problems. For each wind profile shape, a separate power curve is constructed by stepping through a range of wind speeds between the cut-in and cut-out wind speed.

https://doi.org/10.5194/wes-2019-108
Preprint. Discussion started: 17 January 2020

eawe european academy of wind energy
Open Access WIND ENERGY SCIENCE DISCUSSIONS

Parameter	Lower bound	Upper bound
Reel-out force	300 N	5000 N
Reel-in force	300 N	5000 N
Reel-out elevation angle	25°	60°
Pumping length tether	150 m	250 m

Table 5. Optimisation variable limits for the maximisation of the mean cycle power.

Prior to performing the optimisations, the cut-in and cut-out wind speeds need to be determined, which are highly dependent on the wind profile shape. The cut-in limit is assumed to be the smallest wind speed for which, along the whole traction path, steady flight states can be found for the minimum allowable reeling speed. The cut-out limit is determined by the condition that the pumping cycle should contain at least one complete figure-of-eight flight manoeuvre. If the tether is reeled out too fast to complete a single figure-eight, the cut-out wind speed has been exceeded. The original QSM does not resolve the cross-wind flight motion and therefore an additional module has been developed. The kite's motion along the figure-eight is approximated as a transition through steady flight states yielding the duration of such a manoeuvre. Dividing the total duration of the traction phase by the average duration of a figure-eight manoeuvre along the reel-out path yields the number of cross-wind manoeuvres flown. The highest wind speed that still allows flying one complete cross-wind pattern for an elevation angle of 60 degrees is used as the cut-out wind speed.

From the cut-in and cut-out wind speeds for each wind profile shape, the corresponding wind profiles are obtained, see Fig. 17. The cut-in wind profiles have the same wind speed at roughly 80 m indicating that the cut-in criterion is critical at the start of the traction phase for each wind profile. The cut-out profiles exhibit roughly the same wind speed at 300 m. The cut-in and cut-out wind speed characteristics of an AWE system are ambiguous when the heights at which these speeds occur are not specified. For characterising the considered system's cut-in and cut-out wind speed, it would be sensible to use the wind speed at 80 and 300 m, respectively.

Figure 18 shows the idealised cycle trajectories that follow from the optimisations for the representative wind profile shape of cluster 1. The optimal pumping tether length coincides with its upper bound for all wind speeds. The flight trajectory for $v_{100\mathrm{m}}$=10.5 $\mathrm{m\,s^{-1}}$ is the last for which the traction elevation angle coincides with its lower bound. For higher wind speeds, an increased inclination of the reel-out path yields a higher mean cycle power. At roughly $v_{100\mathrm{m}}$=16 $\mathrm{m\,s^{-1}}$, the maximum mean cycle power is reached with the kite completing only one cross-wind pattern. Above 16 $\mathrm{m\,s^{-1}}$ wind speed, the criterion on flying one complete cross-wind pattern is driving the elevation angle to higher values until reaching its upper bound for $v_{100\mathrm{m}}$=19.7 $\mathrm{m\,s^{-1}}$, above which no feasible solution exists.

The computed power curves are shown in Fig. 19. Note that the power is plotted against the wind speed at 100 m, which results in the curves starting at roughly the same wind speed. Plotting the power against the wind speed at 300 m would yield curves that end at roughly the same wind speed. Up to roughly 8.5 $\mathrm{m\,s^{-1}}$, all the power curves show similar values for the

https://doi.org/10.5194/wes-2019-108
Preprint. Discussion started: 17 January 2020

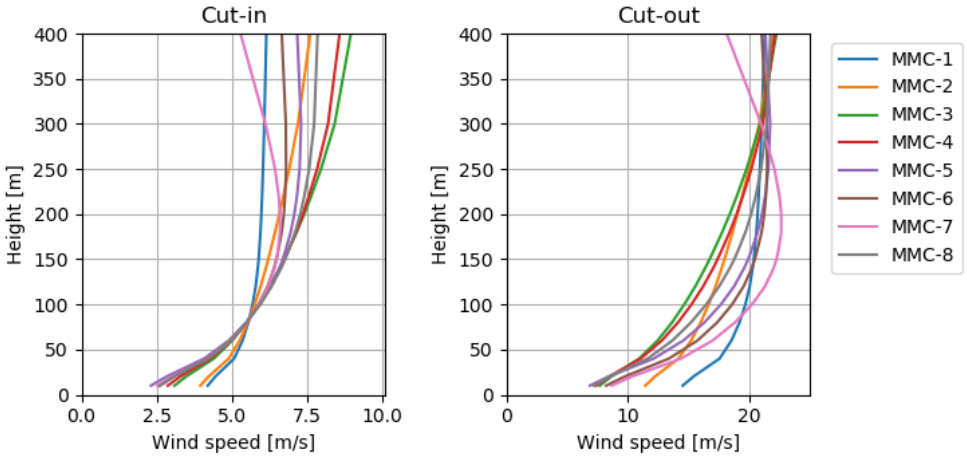

Figure 17. The cut-in (left) and cut-out (right) wind profiles taken from Fig. 11 and adjusted for the cut-in and cut-out wind speeds.

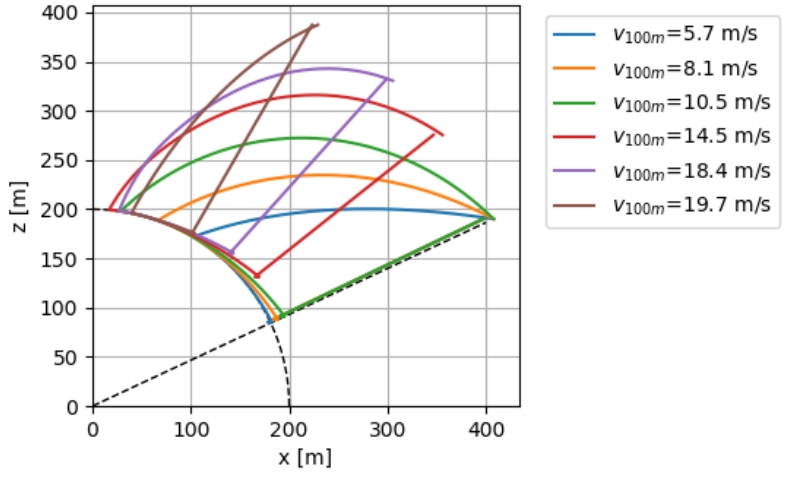

Figure 18. The optimal idealised cycle trajectories for the wind profile shape of cluster MMC-1 for six different wind speeds at 100 m. The angle of inclination of the straight dotted line is the minimum traction elevation angle. The radius of the dotted quarter circle is the constant minimum tether length.

mean cycle power. Above this wind speed, the curves flatten off and become different from one another. The MMC-3 curve shows the lowest maximum mean cycle power and is the first to reach its 100 m cut-out wind speed due to its high-shear wind profile shape. The MMC-7 curve shows the highest maximum mean cycle power and is the last to reach its 100 m cut-out wind speed due to its pronounced low-level jet wind profile shape.

https://doi.org/10.5194/wes-2019-108
Preprint. Discussion started: 17 January 2020

eawe european academy of wind energy
Open Access WIND ENERGY SCIENCE DISCUSSIONS

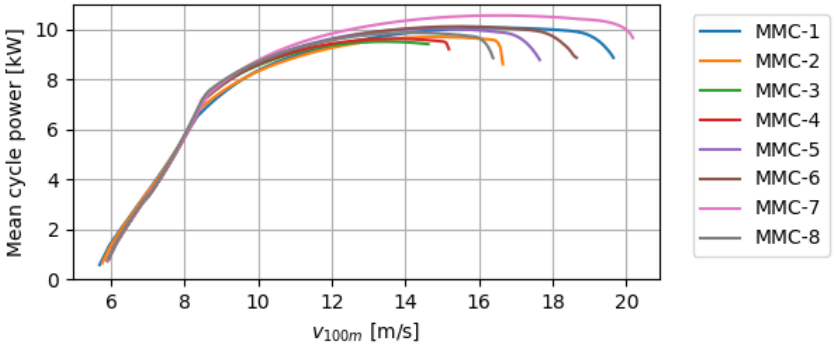

Figure 19. Power curves that are obtained for each wind profile shape using performance optimisations.

5.2 Estimating the Annual Energy Production

The average power output of an AWE system is calculated using:

$$\bar{P} = \sum_{i=1}^{n_{\text{clusters}}} \int_0^{\infty} p_i(v_{\text{norm}}) \cdot P_i(v_{100\text{m}}) \, \mathrm{d}v_{\text{norm}} \tag{3}$$

in which p_i is the wind speed probability of cluster i, P_i is the system's power curve for the wind profile shape of cluster i, v_{norm} is the normalisation wind speed, and the wind speed at 100 m height is given by $v_{100\text{m}} = v_{\text{norm}} \cdot \hat{v}_{i,100\text{m}}$ in which $\hat{v}_{i,100\text{m}}$ is the normalised wind speed of the wind profile shape of cluster i at 100 m height. Multiplying the average power output by the hours in a year gives the AEP estimate.

The integrals in Eq. 3 are solved numerically. Wind speed distributions are constructed for each cluster for the range of wind speeds between the cut-in and cut-out wind speed using 100 bins. This relatively large number of bins is used to mitigate numerical errors. As the 90th percentile wind speed is previously used to normalise the wind profiles and obtain the cluster wind profile shapes, it should also be used to characterise the probability of the clusters and thus for constructing the distributions.

The AEP at the MMC location is evaluated for the MMC and ML cluster representations from Sects. 4.2 and 4.4. Moreover, the number of clusters used for the representation is varied to assess how many clusters are needed for the AEP to converge to a steady value, see Fig. 20. The MMC cluster model trend converges to around 36 MWh for a large number of clusters. For four or more clusters, the AEP error is within a few percent of the converged value and for 14 or more clusters, there is virtually no more variation in the AEP and the steady solution is reached. The error can be mostly explained by the inaccuracy of the cluster wind resource representation, but also by the numerically obtained power curves and inaccuracies in the numerical integration. The MMC cluster model is expected to converge faster than the ML cluster model as it is generated specifically for the evaluated location, which is confirmed by Fig. 20. Note that assumptions in the performance model also affect the convergence, e.g., neglecting the change of wind direction with height is expected to increase the convergence rate. How many clusters to use depends on the application of the AEP calculation, e.g., in a preliminary design optimization, where the

https://doi.org/10.5194/wes-2019-108
Preprint. Discussion started: 17 January 2020

eawe european academy of wind energy
Open Access WIND ENERGY SCIENCE DISCUSSIONS

computational cost is critical, four MMC-clusters is a sensible choice, while for more detailed design studies 14 MMC-clusters would be more suitable.

More than 50 optimizations are used to obtain the power curves, which have a high level of detail. With only a small compromise on the level of detail, half of the number of optimizations can be used, which thus halves the computational cost.

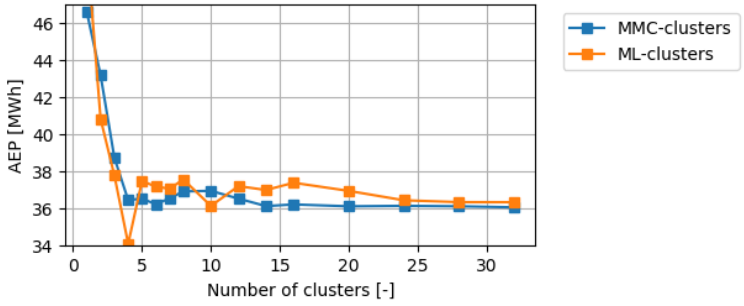

Figure 20. AEP convergence for the MMC location using the MMC and multi-location wind resource representations.

6 Conclusions

We have presented a new methodology to identify a set of characteristic wind profile shapes using clustering for estimating site specific airborne wind resource. The wind resource representation is used for fast AEP calculations for pumping AWE systems. This is necessary because the validity of conventional wind profile parametrisations, such as the logarithmic profile, is limited for the full height range in which these systems operate. Moreover, the availability of new, high-quality, high-resolution reanalysis datasets provides the opportunity for a data-driven approach which allows users to go beyond the use of simple monotonic logarithmic type profiles to characterise site specific resource.

A principal component analysis of wind speed profile data reveals a relatively small number of characteristic wind profile shapes which occur frequently. The offshore MMIJ location shows a concentrated cluster in the principal component space. A similar structure is observed for the onshore MMC location. The samples are, however, still spread out, which indicates that there are a larger variety of wind profile shapes albeit with a much smaller probability of occurrence.

The wide variety of wind conditions in the DOWA wind dataset is reduced to a reasonable number of prevailing wind profile shapes using clustering. The accuracy of the wind resource representation using three or more clusters is higher than the wind resource representation using logarithmic wind profiles. A representation using eight clusters is used to study wind profile patterns for the MMIJ and MMC locations. The resulting wind profile shapes and corresponding statistics are in good agreement with the literature and can directly be linked to meteorological phenomena, in particular, surface layer stability. The ability of this approach to differentiate between atmospheric conditions is confirmed by the resemblance between the resulting sets of wind profile shapes for MMIJ and MMC. This provides confidence that the methodology is suitable for various sites and thus to characterise the wind resource over a larger area. A single set of clusters is generated that is representative for the

https://doi.org/10.5194/wes-2019-108
Preprint. Discussion started: 17 January 2020

eawe european academy of wind energy
Open Access WIND ENERGY SCIENCE DISCUSSIONS

whole DOWA domain and used to analyse the spatial variability of the frequency of occurrence of the clusters. The cluster frequency maps show a clear difference between onshore and offshore wind profile shapes.

The AEP of a flexible-kite, pumping AWE system is estimated using the proposed wind resource representation. For each cluster profile shape, a power curve is obtained using the quasi-steady model, and the corresponding wind speed distribution is obtained from the input wind data. Together they yield each cluster's AEP contribution. For four or more clusters, the AEP error is within a few percent of the converged value and for 14 or more clusters, there is virtually no more variation in the AEP value. Assuming that a four cluster representation provides sufficient accuracy and 25 optimizations are used for generating a single power curve, 100 performance optimizations are required for the AEP calculation against 8760 optimizations per year for a brute force calculation in which for every hour a separate optimization is performed.

The presented methodology has the capability to produce a single set of wind profile shapes that is valid for a large area. Characterising the performance of AWE systems using a standardised set allows comparing the AEP of different AWE concepts for potential installation sites, which makes this methodology a very powerful tool for project developers. In future work we will further investigate how well the methodology is suited for this goal and efforts will be directed towards reaching a consensus on how to characterise the performance of AWE systems. This requires that the role of the performance model in making the AEP calculation is further investigated. We will reassess the modelling assumptions and validate the power curves such that a more definitive answer can be given on how many clusters should be used for certain design studies.

Author contributions. Analysis and preparation of the paper were performed by MS, under the supervision of RS and SJW. PCK provided input on meteorology and data analysis and contributed to writing the result section.

Competing interests. The authors declare that they have no conflict of interest.

Acknowledgements. Without the publicly available Dutch Offshore Wind Atlas by the KNMI, LiDAR observations of the met mast IJmuiden by ECN, and the ERA5 dataset by the ECMWF, this work would not have been possible. The authors would thus like to express their gratitude and support for open data and open science. Mark Schelbergen and Roland Schmehl have received financial support by the project REACH (H2020-FTIPilot-691173), funded by the European Union's Horizon 2020 research and innovation programme under grant agreement No. 691173, and AWESCO (H2020-ITN-642682) funded by the European Union's Horizon 2020 research and innovation programme under the Marie Skłodowska-Curie grant agreement No. 642682.

https://doi.org/10.5194/wes-2019-108
Preprint. Discussion started: 17 January 2020

eawe european academy of wind energy
Open Access WIND ENERGY SCIENCE DISCUSSIONS

References

Bechtle, P., Schelbergen, M., Schmehl, R., Zillmann, U., and Watson, S.: Airborne wind energy resource analysis, Renew. Energ., 141, 1103 – 1116, https://doi.org/https://doi.org/10.1016/j.renene.2019.03.118, 2019.

Brown, A. R., Beljaars, A. C. M., Hersbach, H., Hollingsworth, A., Miller, M., and Vasiljevic, D.: Wind turning across the marine atmospheric boundary layer, Q. J. Roy. Meteor. Soc., 131, 1233–1250, https://doi.org/10.1256/qj.04.163, 2005.

Burk, S. D. and Thompson, W. T.: The Summertime Low-Level Jet and Marine Boundary Layer Structure along the California Coast, Mon. Weather Rev., 124, 668–686, https://doi.org/10.1175/1520-0493(1996)124<0668:TSLLJA>2.0.CO;2, 1996.

Capon, R. A.: Wind speed-up in the Dover Straits with the Met Office New Dynamics Model, Meteorol. Appl., 10, 229–237, https://doi.org/10.1017/S1350482703003037, 2003.

Dörenkämper, M., Optis, M., Monahan, A., and Steinfeld, G.: On the Offshore Advection of Boundary-Layer Structures and the Influence on Offshore Wind Conditions, Bound.-Lay. Meteorol., 155, 459–482, https://doi.org/10.1007/s10546-015-0008-x, 2015.

Duran, P., Basu, S., Meissner, C., and Adaramola, M.: Automated classification of simulated wind field patterns from multi-physics ensemble forecasts, Wind Energy, https://doi.org/10.1002/we.2462, 2019.

Fechner, U.: A Methodology for the Design of Kite-Power Control Systems, Ph.D. thesis, Delft University of Technology, https://doi.org/10.4233/uuid:85efaf4c-9dce-4111-bc91-7171b9da4b77, 2016.

Floors, R., Peña, A., and Gryning, S.-E.: The effect of baroclinicity on the wind in the planetary boundary layer, Q. J. Roy. Meteor. Soc., 141, 619–630, https://doi.org/10.1002/qj.2386, 2015.

Gryning, S.-E., Batchvarova, E., Brümmer, B., Jørgensen, H., and Larsen, S.: On the extension of the wind profile over homogeneous terrain beyond the surface boundary layer, Bound.-Lay. Meteorol., 124, 251–268, https://doi.org/10.1007/s10546-007-9166-9, 2007.

Heilmann, J. and Houle, C.: Economics of Pumping Kite Generators, pp. 271–284, Springer Berlin Heidelberg, Berlin, Heidelberg, https://doi.org/10.1007/978-3-642-39965-7_15, 2013.

Holtslag, M., Bierbooms, W., and van Bussel, G.: Extending the diabatic surface layer wind shear profile for offshore wind energy, Renew. Energ., 101, 96 – 110, https://doi.org/https://doi.org/10.1016/j.renene.2016.08.031, 2017.

Holtslag, M. C., Bierbooms, W. A. A. M., and van Bussel, G. J. W.: Estimating atmospheric stability from observations and correcting wind shear models accordingly, J. Phys. Conf. Ser., 555, 012 052, https://doi.org/10.1088/1742-6596/555/1/012052, 2014.

Kalverla, P. C.: Characterisation of offshore winds for energy applications, Ph.D. thesis, Wageningen University, https://edepot.wur.nl/498797, 2019.

Kalverla, P. C., Steeneveld, G.-J., Ronda, R. J., and Holtslag, A. A.: An observational climatology of anomalous wind events at offshore meteomast IJmuiden (North Sea), J. Wind Eng. Ind. Aerod., 165, 86 – 99, https://doi.org/https://doi.org/10.1016/j.jweia.2017.03.008, 2017.

Kalverla, P. C., Duncan Jr., J. B., Steeneveld, G.-J., and Holtslag, A. A. M.: Low-level jets over the North Sea based on ERA5 and observations: together they do better, Wind Energ. Sci., 4, 193–209, https://doi.org/10.5194/wes-4-193-2019, 2019.

Mahrt, L., Vickers, D., and Andreas, E. L.: Low-Level Wind Maxima and Structure of the Stably Stratified Boundary Layer in the Coastal Zone, J. Appl. Meteorol. Clim., 53, 363–376, https://doi.org/10.1175/JAMC-D-13-0170.1, 2014.

Malz, E., Hedenus, F., Göransson, L., Verendel, V., and Gros, S.: Drag-mode airborne wind energy vs. wind turbines: An analysis of power production, variability and geography, Energy, 193, 116 765, https://doi.org/https://doi.org/10.1016/j.energy.2019.116765, http://www.sciencedirect.com/science/article/pii/S0360544219324600, 2020a.

https://doi.org/10.5194/wes-2019-108
Preprint. Discussion started: 17 January 2020

Malz, E., Verendel, V., and Gros, S.: Computing the power profiles of airborne wind energy systems based on large-scale wind data [Submitted], Renew. Energ., 2020b.

Oehler, J. and Schmehl, R.: Aerodynamic characterization of a soft kite by in situ flow measurement, Wind Energ. Sci., 4, 1–21, https://doi.org/10.5194/wes-4-1-2019, 2019.

Optis, M., Monahan, A., and Bosveld, F. C.: Moving Beyond Monin–Obukhov Similarity Theory in Modelling Wind-Speed Profiles in the Lower Atmospheric Boundary Layer under Stable Stratification, Bound.-Lay. Meteorol., 153, 497–514, https://doi.org/10.1007/s10546-014-9953-z, 2014.

Parish, T. R.: Forcing of the Summertime Low-Level Jet along the California Coast, J. Appl. Meteorol., 39, 2421–2433, https://doi.org/10.1175/1520-0450(2000)039<2421:FOTSLL>2.0.CO;2, 2000.

Park, J., Basu, S., and Manuel, L.: Large-eddy simulation of stable boundary layer turbulence and estimation of associated wind turbine loads, Wind Energy, 17, 359–384, https://doi.org/10.1002/we.1580, 2014.

Pedregosa, F., Varoquaux, G., Gramfort, A., Michel, V., Thirion, B., Grisel, O., Blondel, M., Prettenhofer, P., Weiss, R., Dubourg, V., Vanderplas, J., Passos, A., Cournapeau, D., Brucher, M., Perrot, M., and Duchesnay, E.: Scikit-learn: Machine Learning in Python, J. Mach. Learn. Res., 12, 2825–2830, 2011.

Perez, R. E., Jansen, P. W., and Martins, J. R. R. A.: pyOpt: A Python-Based Object-Oriented Framework for Nonlinear Constrained Optimization, Struct. Multidiscip. O., 45, 101–118, https://doi.org/10.1007/s00158-011-0666-3, 2012.

Peterson, E. W. and Hennessey, J. P.: On the Use of Power Laws for Estimates of Wind Power Potential, J. Appl. Meteorol., 17, 390–394, https://doi.org/10.1175/1520-0450(1978)017<0390:OTUOPL>2.0.CO;2, 1978.

Ranjha, R., Svensson, G., Tjernström, M., and Semedo, A.: Global distribution and seasonal variability of coastal low-level jets derived from ERA-Interim reanalysis, Tellus A, 65, 20 412, https://doi.org/10.3402/tellusa.v65i0.20412, 2013.

Ranneberg, M., Wölfle, D., Bormann, A., Rohde, P., Breipohl, F., and Bastigkeit, I.: Fast Power Curve and Yield Estimation of Pumping Airborne Wind Energy Systems, pp. 623–641, Springer Singapore, Singapore, https://doi.org/10.1007/978-981-10-1947-0_25, 2018.

Shapiro, A., Fedorovich, E., and Rahimi, S.: A Unified Theory for the Great Plains Nocturnal Low-Level Jet, J. Atmos. Sci., 73, 3037–3057, https://doi.org/10.1175/JAS-D-15-0307.1, 2016.

Sommerfeld, M., Crawford, C., Steinfeld, G., and Dörenkämper, M.: Improving mid-altitude mesoscale wind speed forecasts using LiDAR-based observation nudging for Airborne Wind Energy Systems, Wind Energ. Sci., 2019, 1–30, https://doi.org/10.5194/wes-2019-7, 2019.

Van der Vlugt, R., Bley, A., Noom, M., and Schmehl, R.: Quasi-Steady Model of a Pumping Kite Power System, Renew. Energ., 131, 83–99, https://doi.org/10.1016/j.renene.2018.07.023, 2019.